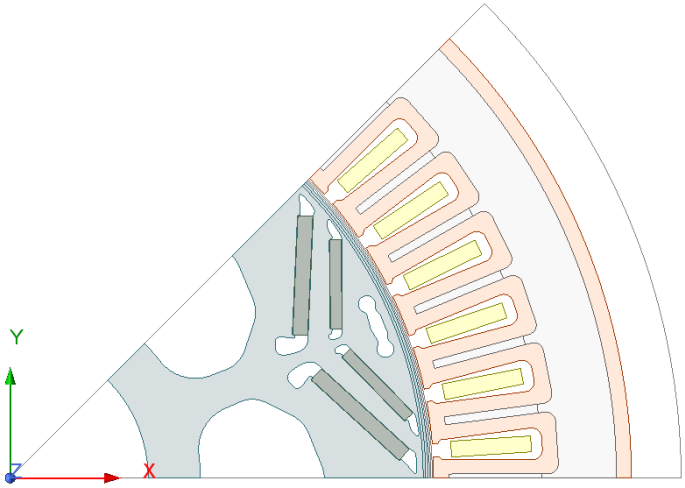

Electric machine loss measurement and modeling

PWM versus sinusoidal feeding

Master's thesis in sustainable electric power engineering and electromobility

PHILIP LISEAU
ARVID MOÄNGE

DEPARTMENT OF ELECTRICAL ENGINEERING

CHALMERS UNIVERSITY OF TECHNOLOGY
Gothenburg, Sweden 2025
www.chalmers.se

Master's thesis 2025

Electric machine loss measurement and modeling

PWM versus sinusoidal feeding

PHILIP LISEAU
ARVID MOÄNGE

CHALMERS
UNIVERSITY OF TECHNOLOGY

Department of Electrical Engineering
Division of Electrical Power Engineering
Chalmers University of Technology
Gothenburg, Sweden 2025

Electric machine loss measurement and modeling
PWM versus sinusoidal feeding
PHILIP LISEAU
ARVID MOÄNGE

Supervisors: Sima Soltanipour and Siavash Sadeghpour, Volvo Cars
Examiner: Torbjörn Thiringer, Electric Power Engineering

Master's Thesis 2025
Department of Electrical Engineering
Division of Electrical Power Engineering
Chalmers University of Technology
SE-412 96 Gothenburg
Telephone +46 31 772 1000

Cover: Electric machine modeled in Ansys Maxwell.

Typeset in LaTeX
Printed by TeknologTryck
Gothenburg, Sweden 2025

Electric machine loss measurement and modeling
PWM versus sinusoidal feeding
PHILIP LISEAU, ARVID MOÄNGE
Department of Electrical Engineering
Chalmers University of Technology

Abstract

As the electrification of the automotive industry continues, the importance of high efficiency electric machines increases significantly. The ability to accurately predict the efficiency and losses in the designing stage is therefore essential. This thesis studied the degradation in magnetic properties in silicon steel strips cut with different widths. These pieces were then used to develop a model to implement manufacturing effects due to cutting in to the electric machine simulations to more accurately model the iron losses. The simulations were fed with both a sinusoidal current and a pulse width modulated voltage feeding to compare the effect of the different feeding types on top of the cutting degradation effect, and compared with each other. For all points simulated, the core losses increased when a layer of degraded material closest to the cut edges of the stator was used, up to 25% with the sinusoidal feeding. For the pulse width modulation case, five different operating points were simulated, showing an increase in core losses of up to 7% when using degraded material. Comparing the effect the feeding types had versus each other, the pulse width modulation fed simulations had core losses up to 258% higher than the sinusoidally fed case. One measurement of the actual machine was compared with the pulse width modulated feeding simulations where the difference between losses was 6.7%, showing promise in the model for the simulated points.

Keywords: iron losses, electric machine, degradation, manufacturing effects, pulse width modulation

Acknowledgements

Firstly, we would like to thank our supervisors, PhD student Sima Soltanipour and Siavash Sadeghpour, for their support and help throughout this project, always being there to help and discuss problems. We also want to thank our examiner, professor Torbjörn Thiringer for his guidance, help and advice during the process, especially in the end. A special thank you goes to Anders Thulin and the Volvo Cars Corporation for the opportunity to complete this interesting thesis work while getting to know the company and industry better.

We would also want to say a big thank you to all the amazing people we have met during these five years at Chalmers. It really would not be the same experience without each and every one of you and all the fun we have had during and outside of school.

Philip Liseau & Arvid Moänge, Gothenburg, June 2025

List of Acronyms

Below is the list of acronyms that have been used throughout this thesis listed in alphabetical order:

AC	Alternating Current
DC	Direct Current
EF	Epstein Frame
EM	Electric Machine
FEM	Finite Element Method
IEC	International Electrotechnical Commission
PI	Proportional Integral
PMSM	Permanent Magnet Synchronous Machine
PWM	Pulse Width Modulation
RMS	Root Mean Square
SPWM	Sinusoidal Pulse Width Modulation
SVPWM	Space Vector Pulse Width Modulation
WLTP	Worldwide Harmonized Light-Duty Vehicles Test Procedure

Nomenclature

A_m	Cross sectional area
B	Magnetic flux density
C_m	Fitting coefficient Steinmetz Equation
f	Frequency
f_r	Frequency modulation index
H	Magnetic field strength
I	Current
$i(t)$	Current flowing over time
i_d	Direct-axis current
i_q	Quadrature-axis current
k_{ec}	Eddy current loss coefficient
k_{ex}	Excess loss coefficient
k_h	Hysteresis loss coefficient
l_m	Length of magnetic path
m_a	Modulation index
N	Number of turns
P_{cu}	Copper losses
P_{trans}	Transmitted power
$P_{loss,tot}$	Total loss
P_s	Specific power loss
$P_{s,deg}$	Specific power loss degradation
R_s	Stator resistance
T	Time of one period
T_e	Torque
$u(t)$	Voltage over time
V	Voltage

w	Width of sample
x	Distance from edge
α	Fitting coefficient Steinmetz Equation
β	Fitting coefficient Steinmetz Equation
μ	Permeability
μ_r	Relative permeability
ω	Angular velocity
Ω	Speed
ρ	Density
η	Efficiency

Contents

1
Introduction

Today sustainability is of great importance and as a result electrification is growing continuously, furthering the development of electric vehicles to combat climate change. Sales of electric vehicles increased by 3.5 million in 2023 compared to 2022, an increase in year-on-year sales of 35% [1]. Electric cars accounted for almost a fifth of all cars sold in 2023 and the weekly sale of electric cars was higher than the annual sale ten years prior [1]. An increase in the efficiency of the electric machine of the vehicle is therefore important to further reduce environmental impact.

1.1 Background

The iron losses in Electric Machines (EM) are difficult to model at higher frequencies and with Pulse Width Modulation (PWM) feeding, where the models currently are restricted. When modeling iron losses, the most common method is to use parameters specific to the steel used in the stator core. These data sheets do not include the manufacturing effects when creating the stator core. The steel materials magnetic properties are degraded during manufacturing from things like heating and cutting. This increases the losses compared to the data sheet values, along with magnetic induction being reduced [2].

Another aspect of the data sheet parameters is that they are derived from sinusoidal flux density [3], whereas PWM is the most common type of feeding of an EM for electric vehicles, providing disturbed sinusoidals [4].

1.2 Previous work

It is clear that degradation has an effect on iron losses, as [5] discovered for the punched cutting method the iron losses increased by 12-24%, which resulted in a decrease of 0.11 percentage points in the total efficiency. The difference in iron loss increase can be due to different material and cutting techniques [5].

Attempts to model the degradation are done in [6], [7] where different functions were used to model the damaged area of a cut sample. In [6] a toroidal core of soft magnetic material was modeled in a Finite Element Method (FEM) model and the width of the degraded area was determined, whereas [7] defined a mathematical equation to approximate how the relative permeability in a cut sample is changed. Neither study applied their results to an EM.

A previous master's thesis investigated the effect of PWM feeding to an EM, where the increased percentage difference between sinusoidal feeding and PWM feeding were 120 to 750 % [5]. The method used was extracting magnetic properties from PWM fed measurements in an Epstein Frame. These new material magnetic properties were then incorporated into a FEM based program Ansys Maxwell, which then was fed with sinusoidal feeding. This thesis will instead build a PWM circuit with inverter and current controller to more accurately simulate PWM.

1.3 Purpose

The purpose of this thesis is to model the iron losses due to manufacturing effects and due to both sinusoidal and PWM feeding. To realize this, the following objectives were set:

- Calculate the degradation effect of cutting the material from measurements on rectangular strips.
- Model the degradation effects in a FEM-based software.
- Model the effect of PWM feeding in a FEM-based software.
- Compare losses from simulations with non-degraded material to simulations with degraded material for both sinusoidal and PWM feeding.
- Measure the losses in an EM and compare them to degraded material PWM simulations.

2

Theory

2.1 Manufacturing effects

Electrical machines are built with laminated electrical sheets that are joined together. The unprocessed electrical sheets have magnetic properties that are worsened as the electrical sheet is cut and processed [8], called degradation or manufacturing effects. The process of cutting is usually the largest part of the degradation effect [9]. The type of cutting used is significant for the level of degradation of the magnetic properties. The method most commonly used for mass-production of EMs is punching [10]. Punching means that the material is stamped to the desired shape with a tool that is geometry specific. This leads to the initial cost being high, but as larger-scale production is done, the total cost is lower compared to other cutting methods. An advantage with the punching method is that there is no thermal stress applied during punching. However, there will be mechanical stress. This degradation of magnetic properties impede the permeability and lower the flux density for a specific field strength, increasing core losses in an EM [10].

2.2 Measurement methods

There are several different techniques to measure magnetic properties in electrical steel sheets. This project has narrowed its scope to just look at the most common method, the Epstein Frame procedure. Magnetic properties include, but are not limited to, the magnetic field strength H, the magnetic flux density B, and the specific power loss P_s. Ampere's law is used to calculate the magnetic field strength

$$H(t) = \frac{N_1 i(t)}{l_m} \tag{2.1}$$

where N_1 is the number of turns around the sample, $i(t)$ is the current flowing through the winding over time and l_m is the length of the magnetic path. The voltage induced over the secondary winding u_2 can be used together with Faraday's law to calculate the flux density as

$$\frac{dB}{dt} = -\frac{u_2(t)}{N_2 A_m} \Rightarrow B(t) = -\frac{1}{N_2 A_m} \int_0^t u_2(t)\, dt \tag{2.2}$$

where N_2 is the number of turns on the secondary side of the windings and A_m is the cross-sectional area of the electrical steel sheet. Additionally, the specific power loss of the material P_s can be calculated as

$$P_s = \frac{f}{\rho} \int_0^T H \, dB \tag{2.3}$$

where f is the frequency, ρ the density of the material, T is the time period, H is the magnetic field strength and dB is the magnetic flux density varying with time.

2.2.1 Epstein Frame

The Epstein Frame (EF) has four coils, formed as a square, with primary and secondary windings connected in series [11]. Steel strips are positioned in the square with overlapping edges, which requires the number of samples to be a multiple of four. Due to the overlapping edges, leakage flux occurs during testing. The EF measurements follow the International Electrotechnical Commission's (IEC) standard IEC 60404-2, which states that the strips should be 30 mm in width and between 280 mm and 320 mm in length [4].

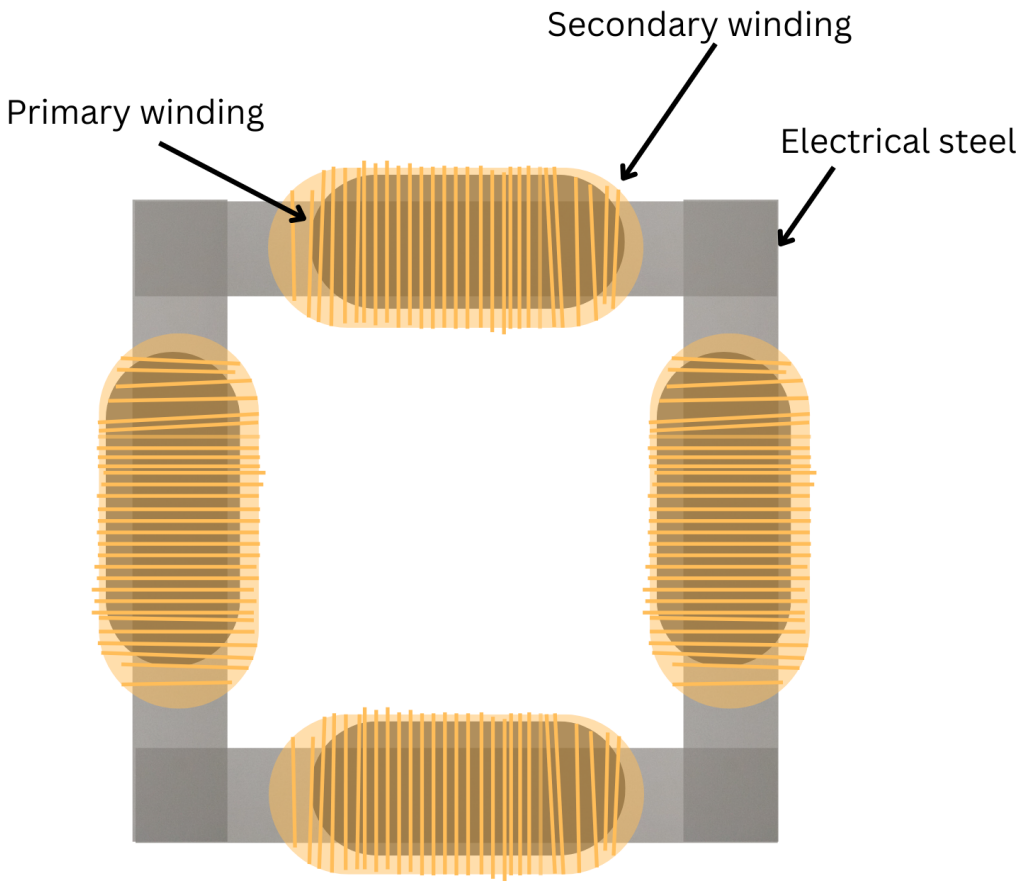

Figure 2.1: Epstein Frame geometry from top perspective

2.3 Pulse Width Modulation

Instead of using sinusoidal feeding, a switching method commonly used for electric machines in propulsion is Pulse Width Modulation (PWM). Sinusoidal PWM (SPWM) is shown in Figure 2.2. The principle of SPWM is to compare a triangular carrier wave with a reference sinusoidal wave [12]. The way to modulate the carrier wave is by changing the switching frequency compared to the reference wave frequency

$$f_r = \frac{f_{carrier}}{f_{reference}} \tag{2.4}$$

and to change the amplitude of the carrier wave

$$m_a = \frac{\hat{V}_{reference}}{\hat{V}_{carrier}} \tag{2.5}$$

where $\hat{V}_{reference}$ is the peak reference voltage and $\hat{V}_{carrier}$ is the peak carrier voltage. The values of m_a are usually between 0 and 1, values over 1 are called overmodulation, which could lead to unwanted harmonics in the PWM signal [13].

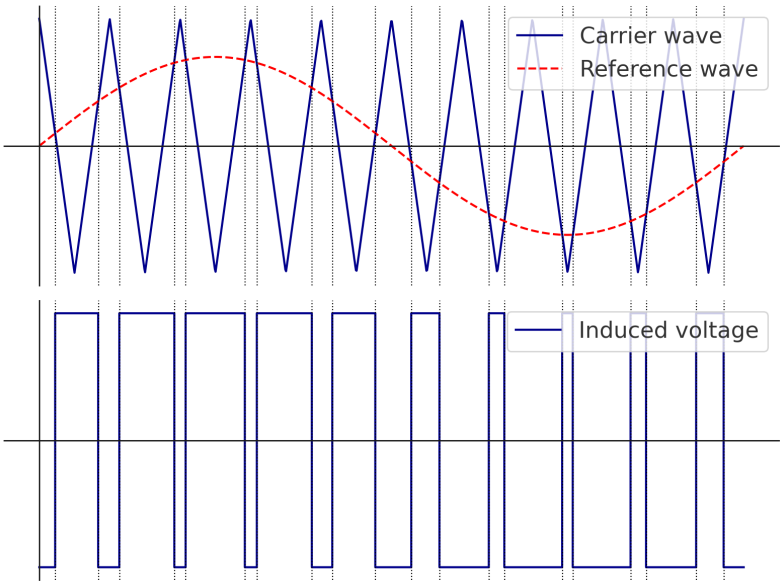

Figure 2.2: The carrier and reference wave and the resulting PWM induced voltage

2.3.1 Space Vector PWM

The Space Vector PWM (SVPWM) principle is that six non-zero base vectors $\overrightarrow{V_{s1}}$, $\overrightarrow{V_{s2}}$,..., $\overrightarrow{V_{s6}}$ of a half bridge three-phase inverter [12], are used to synthesize the output reference voltage instead of using a carrier wave, as shown in Figure 2.3. v_{ref} is the output voltage required and the relationship between output voltage and input voltage in the $\alpha - \beta$ frame for one switching cycle is

$$\int_0^{T_s} v_{ref} dt = \int_0^{T_a} v_a dt + \int_0^{T_b} v_b dt \tag{2.6}$$

In order to lower harmonics in the signal, two more vectors, $\overrightarrow{V_{s7}}$ and $\overrightarrow{V_{s8}}$, are inserted, which both are zero voltage space vectors.

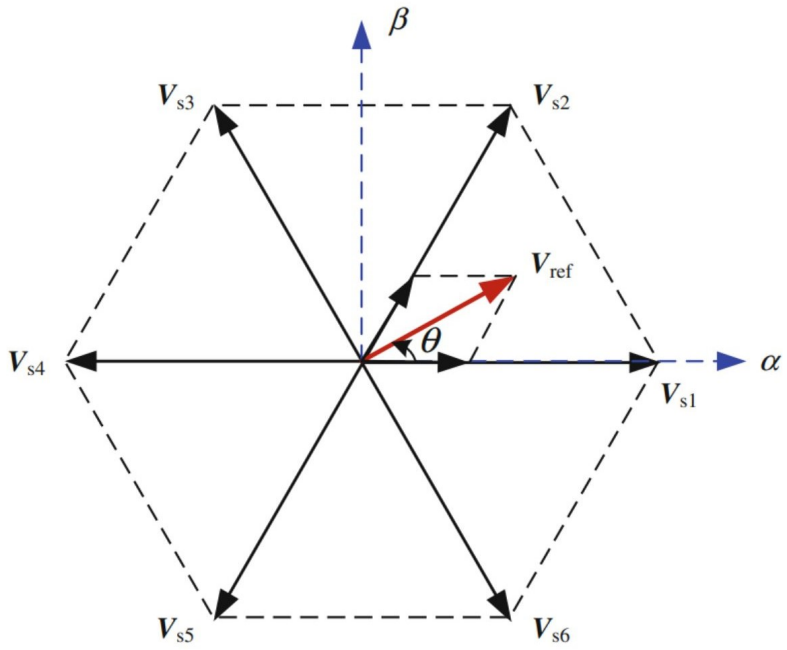

Figure 2.3: Voltage base vectors synthesizing v_{ref}

The main benefit of SVPWM compared to SPWM is the utilization of the DC voltage. For the SPWM case, the highest DC voltage utilization rate is 0.866, whereas for SVPWM the highest DC voltage utilization rate is 1.155 [12]. This can also be achieved by using SPWM with a zero-sequence addition to the reference waves [14].

2.4 Losses in electrical machines

The losses in an EM can be divided into categories depending on where they occur, most common being separation into mechanical, copper, and iron losses. The mechanical losses include bearing losses and windage losses, that are hard to model [15], whereas the copper losses are calculated by

$$P_{cu} = 3R_s I_{rms}^2 \tag{2.7}$$

where R_s is the stator resistance and I_{rms} is the rms value of the current.

2.4.1 Iron losses

The iron losses occur as a result of flux alternating in ferromagnetic material, such as the stator and rotor core, and is why they are sometimes referred to as core losses.

They can be categorized into three different groups: hysteresis, eddy current, and excess losses. The iron losses are especially difficult to model, as they are not easily measured. The modeling is more of an engineering method to fit the real life iron losses [16].

2.4.1.1 Hysteresis losses

Hysteresis losses are related to the magnetization and demagnetization of the core. When a ferromagnetic material is slowly magnetized with an increasing H-field and then demagnetized with a negative H-field, the path for the magnetization curve does not align [17]. The area enclosed by the magnetization curve (hysteresis curve) is equal to the energy loss for each cycle of magnetizing and demagnetizing [17]. For PWM feeding, smaller hysteresis loops are also present inside the larger hysteresis loop. These minor loops occur due to the switching on and off of the magnetic field [5]. When the switching frequency increases, the area of these minor loops decreases [5], but the amount of minor loops increase, as can be seen in figure 2.5.

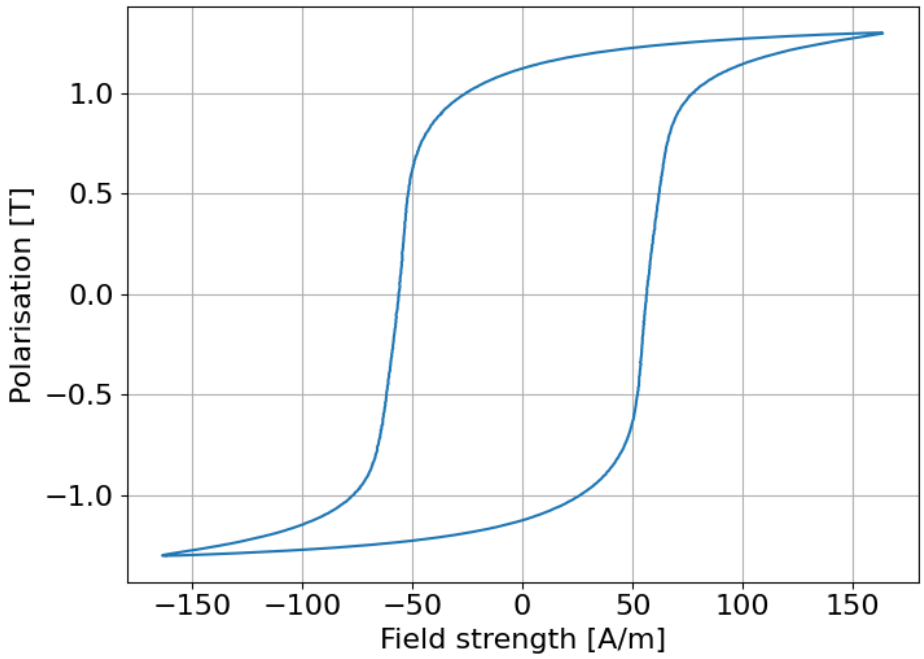

Figure 2.4: Example of hysteresis curve with sinusoidal feeding

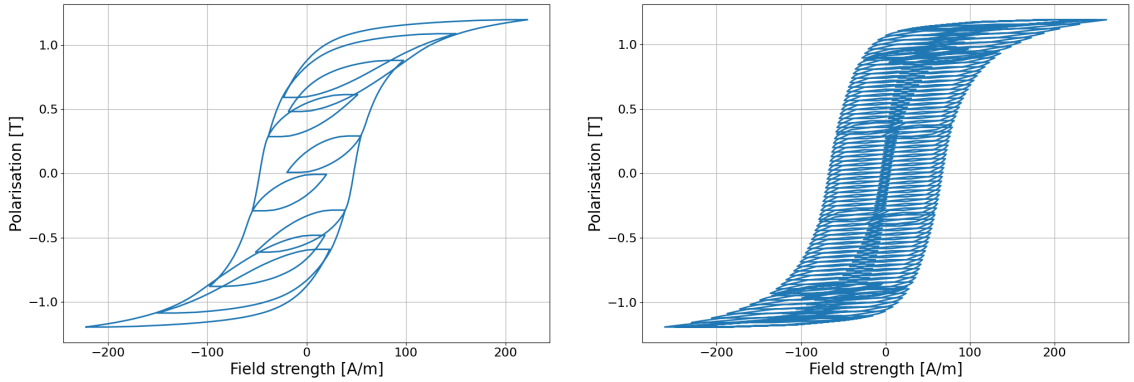

(a) Hysteresis curve of PWM feeding when switching frequency is 9 times the fundamental frequency (f_r=9)

(b) Hysteresis curve of PWM feeding when switching frequency is 199 times the fundamental frequency (f_r=199)

Figure 2.5: Example of hysteresis curves with PWM feeding, where minor loops appear

2.4.1.2 Eddy current losses

Eddy current losses occur due to the electrically conductive material being exposed to a changing magnetic field, inducing voltages and currents, according to Faraday's law [18]. The induced currents in the material, eddy currents, circulate on the surface and counteract the magnetic field that made the induced current occur [18], with power being dissipated as heat due to the resistivity of the material [19].

2.4.1.3 Excess losses

Excess losses are the losses when calculating the total magnetic losses and subtracting the eddy current and hysteresis losses. These losses occur because the loss modeling estimates the eddy current losses wrongly and does not predict the frequency dependence correctly [20]. These losses are referred to as an anomaly of the eddy current losses and are often called the "anomalous losses" [20].

2.4.1.4 Iron loss modeling

There are numerous methods for modeling iron losses. The model used in the FEM program Ansys Maxwell and in this thesis is based on a group of models called the Steinmetz equation

$$P_s = C_m f^{\alpha} \hat{B}^{\beta} \tag{2.8}$$

where P_s is the specific power loss, $\hat{B}$ is the peak flux density of the material, f is the fundamental frequency and α, β and C_m are fitting coefficients and are all determined by measurements. The Steinmetz model has been modified to a General Steinmetz equation and an Improved General Steinmetz equation. However, the problem with the modified versions of the Steinmetz equation is that the fitting coefficients are varying with frequency, making it problematic to find coefficients applicable for all frequency ranges and signals with high harmonic content.

The model used in Ansys Maxwell is called the Bertotti model and builds on the principle of separating the iron losses in three categories: hysteresis loss, eddy current loss and excess loss. The total iron loss becomes

$$P_s = P_h + P_{ec} + P_{ex} = k_h f B_m^2 + k_{ec} f^2 B_m^2 + k_{ex} f^{1.5} B_m^{1.5} \tag{2.9}$$

where k_h, k_{ec} and k_{ex} are fitting coefficients for the hysteresis-, eddy current- and excess losses. When the frequency approaches 0, it can be assumed only the hysteresis losses are present and that the hysteresis losses are proportional to the area of the hysteresis loop of the material.

Based on Maxwell's equations, the eddy current coefficient k_{ec} can be calculated as

$$k_{ec} = \frac{\sigma \pi^2 d^2}{6\rho} \tag{2.10}$$

where σ is the conductivity, ρ is the density of the material and d is the thickness of the electrical steel.

2.5 Degradation model

Since degradation due to manufacturing of sheets originates at the cut edge and propagates inward into the material [21], functions were developed to model this behavior by calculating the relative permeability, μ_r, and the specific power loss, P_s, as functions of the distance from the cut edge.

2.5.1 Relative permeability modeling

The relative permeability of a material is governed by the magnetic flux density, which tends to degrade near cut edges due to localized structural disturbances. Consequently, the relative permeability decreases in proximity to the cut edge. Measuring the exact flux density at a specific point inside the material is practically impossible. Instead, what's typically measured is the average flux density over the entire sample.

In [7], a model was proposed to describe the relative permeability as

$$\mu_{r,\text{calculated}}(x, B) = \mu_{r,\text{pristine}}(B) \cdot f(x) \tag{2.11}$$

where the degradation function is defined as

$$f(x) = 1 - ae^{-bx} - ce^{-dx} \tag{2.12}$$

Here, x is the distance from the cut edge, and $\mu_{r,\text{pristine}}(B)$ represents the relative permeability of the undamaged material, dependent on the flux density B.

Because the measured flux density, B_{measured}, is an average over the width of the sample, it can be expressed as

$$B = \frac{1}{w} \int_0^w \mu_0 \mu_r(x, B) H \, dx \tag{2.13}$$

where w is the sample width, μ_0 is the vacuum permeability, and H is the magnetic field strength. Substituting (2.11) into (2.13) yields

$$B = \frac{\mu_0 \mu_{r,\text{pristine}}(B) H}{w} \int_0^w f(x) \, dx \tag{2.14}$$

2.5.2 Specific power loss modeling

The specific power loss P_s of a material describes its loss in relation to the weight or volume of the material. More cuts in a single strip degrades the material, increasing its specific power loss compared to the uncut material, and can be described as a unitless scale factor $P_{s,deg}$ where

$$P_{s,deg} = \frac{P_{cut}}{P_{uncut}} \tag{2.15}$$

and P_{cut} is the specific power loss for a cut sample and P_{uncut} is the specific power loss for an uncut sample, both that vary with different field strengths and frequencies. This makes a series of points for $P_{s,deg}$ for each B value and frequency that depend on the width of the cut sample that can be curve-fit towards with

$$P_{s,deg}(x) = a_p \cdot e^{-b_p x} + c_p \tag{2.16}$$

where a_p, b_p and c_p are fitting coefficients and x is half the width of the strip, corresponding to the distance from the cutting edge.

3
Methods

3.1 Measurement

The physical measurements were done to investigate the effects of degradation on the material in sheet-form and to correlate the results to the iron losses in the built machine. The tests were both done using sinusoidal feeding and PWM feeding.

3.1.1 Sheet testing

The electrical steel strips were measured in an Epstein Frame from Brockhaus with software from Brockhaus Measurements. The winding configuration in the EF has different limitations in terms of frequency, field strength and flux density [22], which are described in Table 3.1.

Table 3.1: Range of operation for the EF

EF frame	Frequency f [Hz]	Flux Density B [T]	Field Strength H [A/m]
700	3-150	0.001-2	5-30 000
200	150-2 000	0.005-1.8	0-5 000
60	1 000-5000	0.001-2	5-3 000
20	2 500-20 000	0.001-2	0-1 000

The material used was a 27 mm silicon steel, cut in the rolling direction with a punched cutting technique. The testing was done in the EF with 16 pieces of lamination steel. For every frequency listed in Table 3.2, there were five tests done. Every test started at a high flux density to avoid remanent magnetization, and was stepped down with 0.1 T steps down to 0.1 T. The changes in the starting values of magnetic field strength were due to the fact that losses were very large at higher B-values for higher frequencies, leading to heating that could sabotage the EF by melting different parts. B_{start} was chosen as the higher value for the measurement because if the opposite was chosen such that the highest B-value would end the experiment, the material would still be magnetized, which leads to remanence. The changes in windings in the EF were chosen in accordance with EF recommendations of frequency span of different windings. These five data sets from each frequency were then compared to each other and the averages of the five data sets to discover outliers, which were removed. The outliers were defined such that any value that differed by more than 2% from the average were removed and if the whole data set had a sum of differences to equal larger than 5%, the whole data set was removed.

Table 3.2: Different start values for B-field over different frequencies

Frequency [Hz]	B_{start} [T]	B_{step}	B_{end} [T]	EF frame
50	1.9	0.1	0.1	700
100	1.8	0.1	0.1	700
200	1.4	0.1	0.1	200
400	1.4	0.1	0.1	200
700	1.4	0.1	0.1	200
1000	1.1	0.1	0.1	60
2500	1.1	0.1	0.1	60
5000	0.9	0.1	0.1	20
10000	0.7	0.1	0.1	20

3.1.1.1 Different cuts

To get a model of degradation, the material was cut into different widths. The material was cut in the rolling direction and then put together again to investigate the degradation due to cutting material. With each cut, the distance from the edge to the cut decreased, making it feasible to model degradation with distance from the edge as the variable.

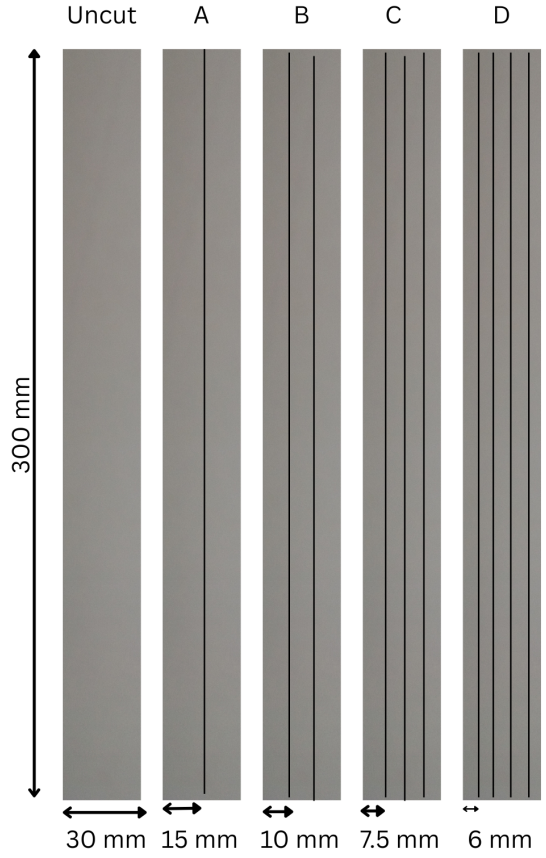

Figure 3.1: Investigated strips

As it is difficult to get the degradation in each point of the material, a simplification

was made to take the average degradation from the cutting edge, where distance to cutting edge is half the distance from cutting edge to the last cut

$$x = \frac{w}{2} \tag{3.1}$$

The name "uncut" is not entirely accurate as the sheets are cut down to fit with the IEC standard IEC60404-2. However, "uncut" refers to sheets with no additional internal cuts. This served as a point of reference to compare the number of cuts and how the closer the distance to the cutting edge affects degradation. It should be noted that this introduces some error, since there is degradation on the outer edges of the so-called "uncut" sheet.

Table 3.3: Number of cuts and distance to cutting edge x for the different samples

Sample	Uncut	A	B	C	D
Number of cuts	0	1	2	3	4
Width w [mm]	30	15	10	7.5	6
Distance from edge x [mm]	15	7.5	5	3.75	3

3.1.2 Machine testing

To measure whether the results from degradation more closely represent the real machine, testing on an actual machine was conducted. The setup was a Direct Current (DC) supply connected to the grid which was connected to an inverter. The inverter converted the DC into Alternating Current (AC) and then fed into the EM, with SVPWM feeding. The EM was coupled with a coolant, which had a temperature sensor. On the actual machine, there were current, voltage, rotor position and flow rate sensors. All this data was collected and sent to a computer which was connected with the inverter through a controller. The program used to simulate the driveline was CANalyzer.

As the test rig for the machine was not yet fully functional to run under load, the tests were done at no-load. The tests were done at every 1000 rpm speed, where the DC voltage supply increased in steps of 210 V, 290 V, 380 V and 460 V. Then measurements were done at each step of voltage. When 5000 rpm was reached, the lowest voltage, 210 V, was removed due to problems when operating in the field weakening region. This was done until 12 000 rpm was reached. The mechanical power drawn of a machine is

$$P_{trans} = T_e \cdot \omega \tag{3.2}$$

where P is power, T_e is torque and ω is the angular frequency. Due to that the EM being run at no-load, $T_e = 0$, all the input power is equal to the losses of the machine. All of these losses are however not iron losses, as when the machine is spinning, friction losses occur which increase at higher speeds. Even during no-load operation, small currents flow through the machine, leading to losses in the windings. To ensure these don't get included in the comparison with simulation, the winding losses were subtracted from the power flowing into the machine, by (2.7). The iron losses were then compared at two operating points to a simulation of a degraded

machine with PWM feeding at these two points, as the feeding into the machine was PWM.

3.2 Modeling

Degradation starts at the cut edge and gradually spreads into the material, with a reduced severity. To capture this effect, models were created to describe how the relative permeability, μ_r, and the specific power loss, P_s, change with distance from the cut edge. The measurements collected data only down to a strip of 6 mm width, meaning 3 mm from the cutting edge to the center, and therefore the models had to be able to extrapolate values for smaller distances.

3.2.1 Relative permeability model

To keep the model physically reasonable, some constraints are necessary. Since the permeability should approach the pristine value far from the cut edge and never drop below zero near it, the parameters in $f(x)$ from (2.12) must satisfy

$$0 < a + c < 1 \tag{3.3}$$

Additionally, both b and d must be greater than zero to ensure that the permeability decreases near the edge. To avoid overlap between the exponential terms, b is set to always be smaller than d, which gives

$$0 < b < d \tag{3.4}$$

The expression in (2.14) was used to fit the function $f(x)$ using a least squares method in Python. Since the expression depends on the magnetic flux density this was done for each B value at each frequency generating a range of parameters. In Figure 3.2 an example is shown of how the permeability in a 30 mm wide strip cut at both edges is affected at 0.5 T and 50 Hz.

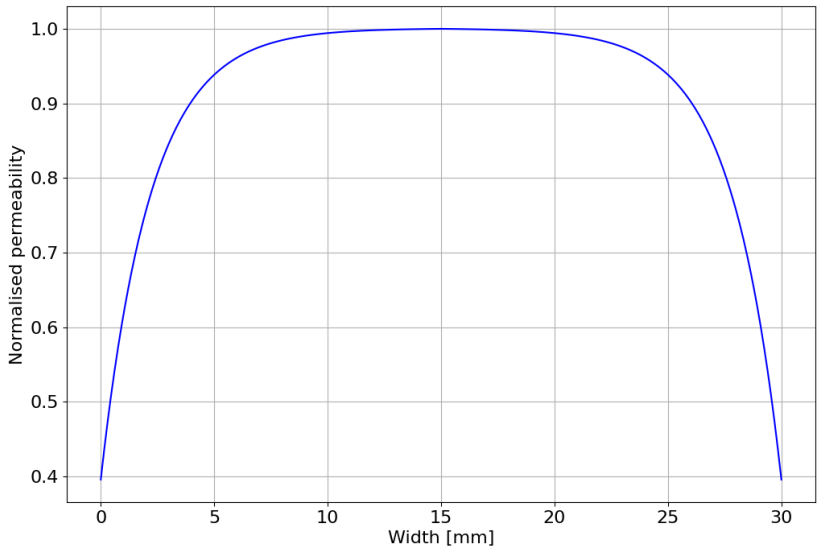

Figure 3.2: Normalized permeability in a 30 mm wide strip with cuts at both edges, at 0.5 T and 50 Hz

The parameters for (2.12) over all B values at 50 Hz are shown in Figure 3.3.

To compare the model with measurements, the calculated relative permeability was determined using

$$\mu_{r,\text{calculated}} = \frac{\mu_{r,\text{uncut}}}{w} \int_0^w f(x), dx \tag{3.5}$$

resulting in a curve that could be compared with the measured values.

3.2.2 Specific power loss model

The degradation factor $P_{s,deg}(x)$ from (2.16) does not have any real physical linking, instead it is purely mathematically fitted towards a series of points. Each measured strip created a point of degradation varying with the distance from cut edge that the model was fit to with the least squares method. In Figure 3.4 the model for $B = 0.5$ T at 50 Hz is shown in relation to the measured points.

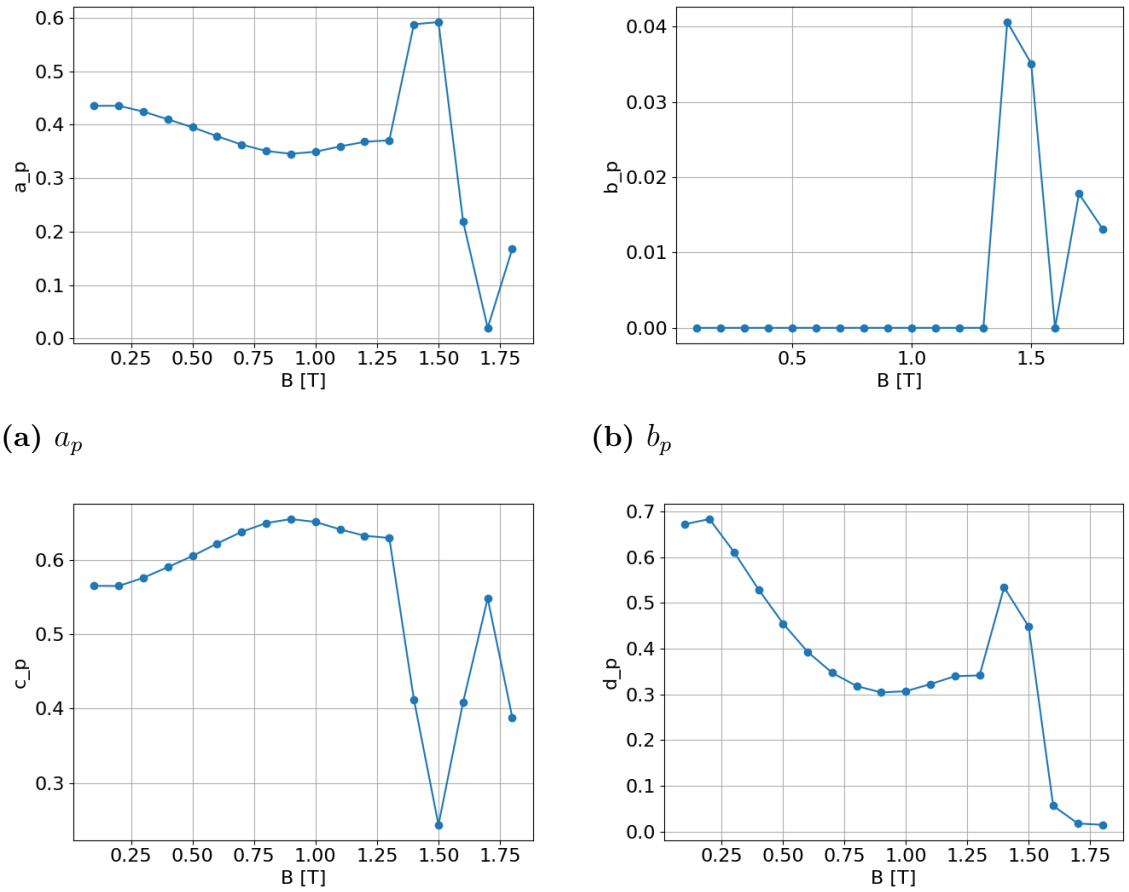

(a) a_p **(b)** b_p

(c) c_p **(d)** d_p

Figure 3.3: Parameters a_p, b_p, c_p, and d_p for different flux densities at 50 Hz

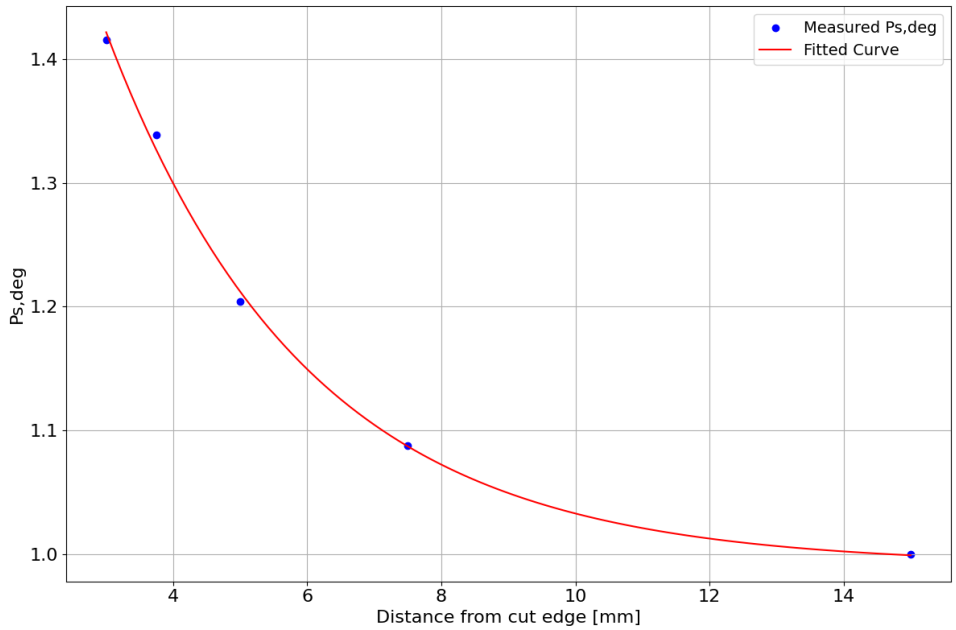

Figure 3.4: Curve fit of $P_{s,deg}$ from measured points for $B = 0.5$ T at 50 Hz

Since the degradation varies with flux densities and frequency, the fitted model had different parameters for each condition. In Figure 3.5 the parameters are shown versus flux density at 50 Hz.

3.3 Simulation

The model was built in the FEM-based program Ansys Maxwell. To simulate PWM feeding, an inverter with SPWM was built in Ansys Simplorer and connected through Ansys Twin Builder.

3.3.1 EM model

The machine modeled was a Permanent Magnet Synchronous Machine (PMSM) with eight poles. Since the machine's poles are symmetric, an eighth of the machine could be represented, reducing the computational time. The geometry built in Ansys Maxwell is shown in Figure 3.6.

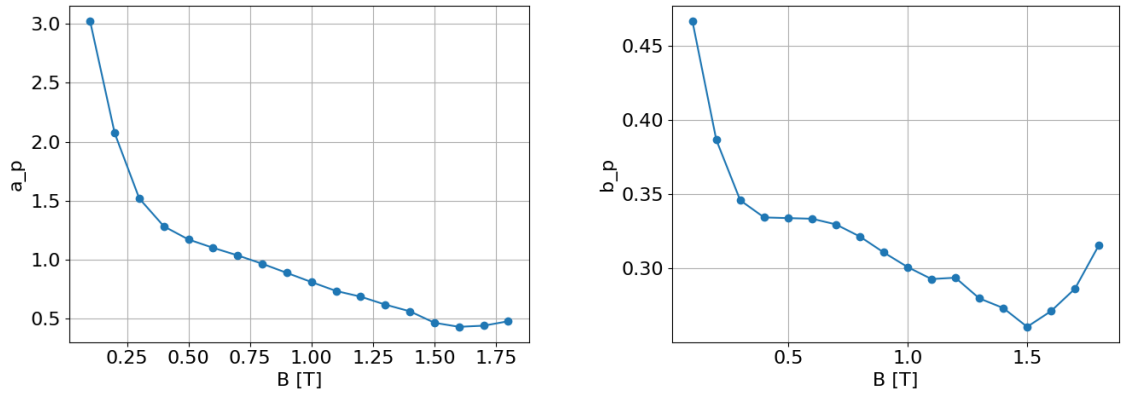

(a) a_p **(b)** b_p

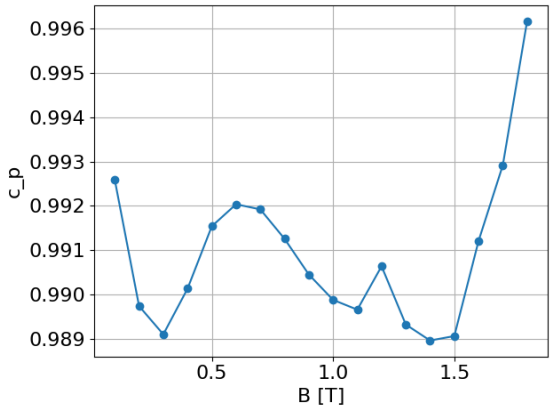

(c) c_p

Figure 3.5: Parameters a_p, b_p, and c_p for different flux densities at 50 Hz

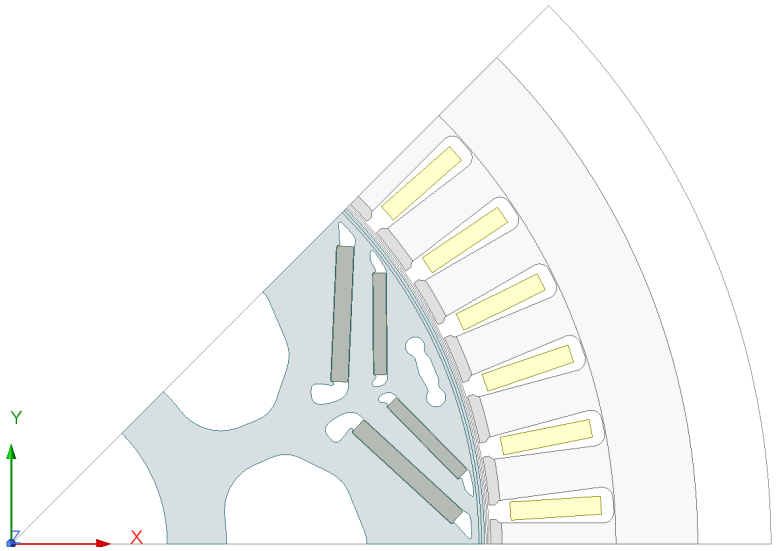

Figure 3.6: Geometry of EM-model simulated in Ansys Maxwell

The EM was modeled using general parameters that are disclosed in Table 3.4.

Table 3.4: General parameters for the modeled EM in Ansys Maxwell

Parameters	Value
Stator Outer Diameter	250 mm
Stator Inner Diameter	170.4 mm
Rotor Outer Diameter	168.2 mm
Rotor Inner Diameter	55.5 mm
Active Length	119.34 mm
Number of Poles	8
Number of Slots	48

3.3.2 EM model with degraded material

To simulate the degradation the EM is affected by, a model with a layer of degraded material in the stator core was made, as shown in Figure 3.7. Since the layer was modeled by section 3.2 it was chosen to use one degradation layer of 3 mm. The rest of the stator core was left as non-degraded material. The degradation model was only implemented in the stator, to focus on the iron losses in the stator. To get comparisons with the non-degraded machine that are under equal conditions (similar mesh distances in each part of the machine for instance), the degraded model was used for both simulations. When non-degraded was simulated, the degraded area was kept as the same material as the rest of the stator.

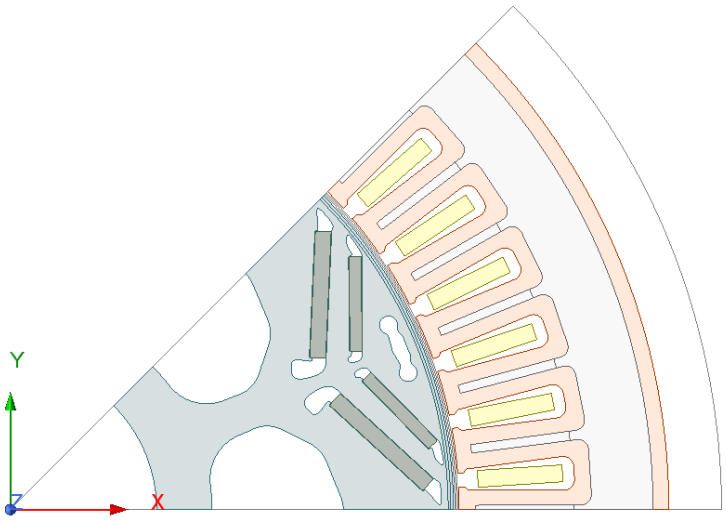

Figure 3.7: Geometry of EM-model with a degradation layer simulated in Ansys Maxwell

3.3.3 SPWM modeling

To model the SPWM feeding of the current to the EM, an inverter, current controller and SPWM generator was built in Ansys Simplorer. The Proportional Integral (PI) controller for the current controller were blocks from Simplorer. The inverter built was a three-legged inverter with ideal switches. The inverter losses were then not considered as it is only the signal into the machine that was looked at. The circuit built in Ansys Simplorer was then connected to the EM using Ansys Twin Builder to connect Ansys Simplorer to Ansys Maxwell.

The full circuit is shown in figure 3.8, which might be difficult to see the different small parts in the circuit. This is why the circuit is zoomed in at the different interesting parts, shown in figure 3.9.

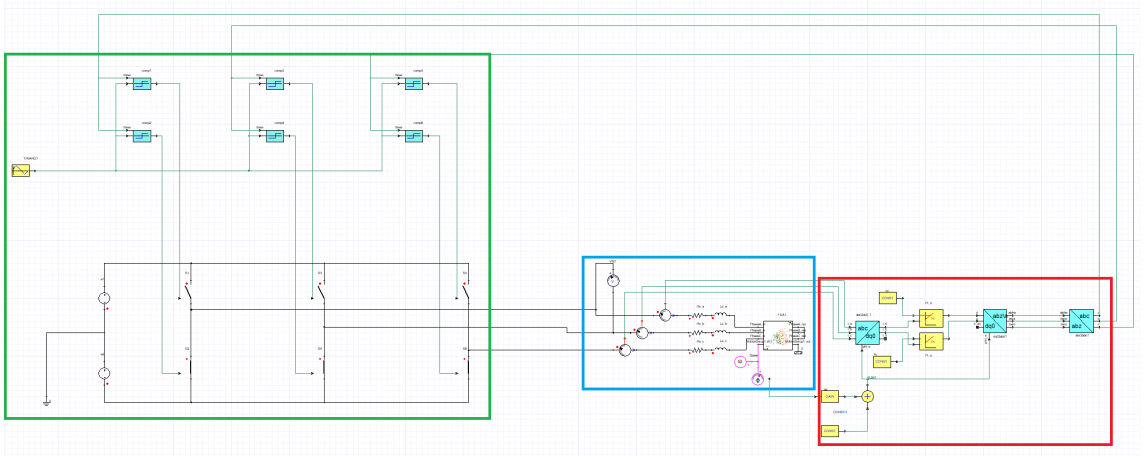

Figure 3.8: Full circuit of the SPWM model with inverter, current controller and EM

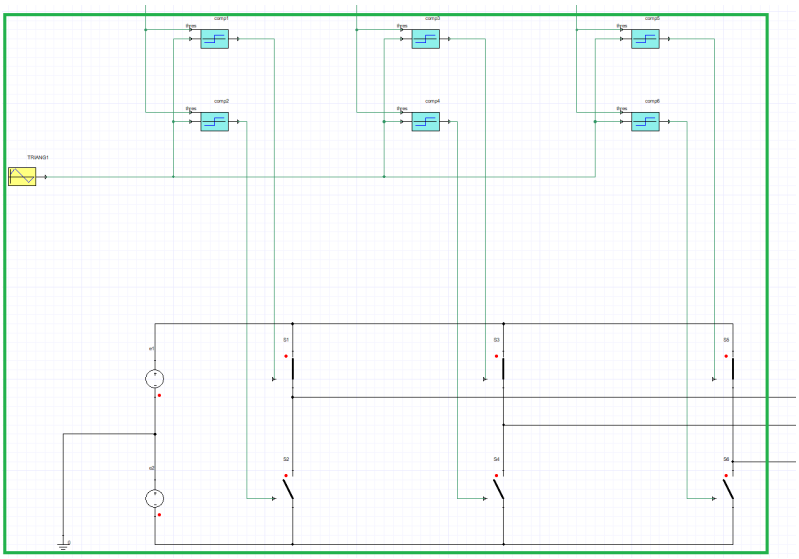

(a) SPWM generation and inverter

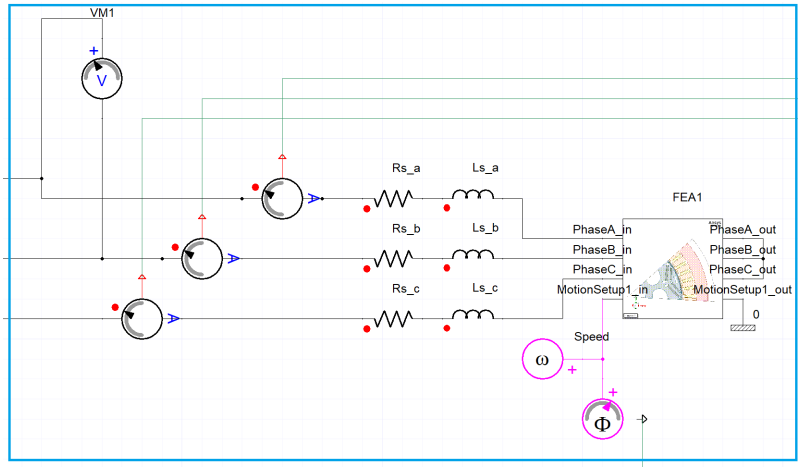

(b) Current feeding to the EM

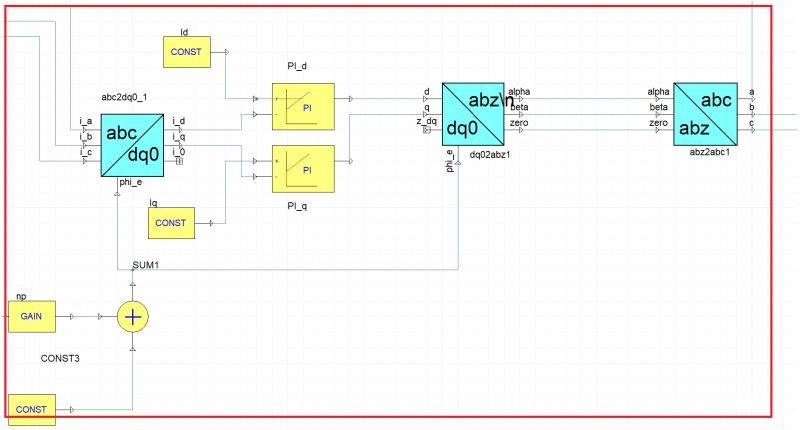

(c) Current controller

Figure 3.9: The whole circuit zoomed in to three parts

3.3.4 Simulation method

3.3.4.1 Sinusoidal feeding

The actual simulation was done after each step in sections 3.3.1-3.3.3 were done, where the first was sinusoidal feeding when the EM without degradation was built. The method used was feeding different i_d and i_q current sweeps to the machine, described in Table 3.5. These different currents fed into the machine generated inductance in both d and q direction, which in turn with post processing made a torque-speed map. To generate these different currents, the Optimetrics setting in Ansys Maxwell was used. This mapping was all done at 1000 rpm and then extrapolated to all the different speeds.

Table 3.5: i_d and i_q sweep

	i_d [A]	i_q [A]
start	0	0
stop	-700	700
step	-50	50

This resulted in a new Table of i_d and i_q currents that corresponded to different operating points. The simulation was then rerun with these new currents for the chosen speeds where the material was measured. This led to simulation results at 23 different torques at 6 different speeds. This was done to more accurately simulate the losses in Ansys Maxwell as the first sweep where the $T - \Omega$ map was done, the losses were estimated at 1000 rpm and extrapolated to higher speeds. This rerun of the simulation ensures a more accurate loss map for the same $T - \Omega$ map.

To more accurately simulate the material, the material was designed differently for each frequency by inserting measured $B - H$ curves and calculating Bertotti coefficients from the specific power loss and flux densities. For the nondegraded simulations, the measurements used were the uncut steel, whereas for the degradation the curves and coefficients were created with the modeling in section 3.2. This was implemented during the rerun of the simulation, which more accurately simulated losses.

To calculate the total transmitted power equation 3.2 was used. In order to calculate the efficiency, the copper losses are calculated by (2.7) and added to the iron losses, then subtracted from the transmitted power and then divided by the transmitted power.

$$\eta = \frac{P_{trans} - P_{loss}}{P_{trans}} \tag{3.6}$$

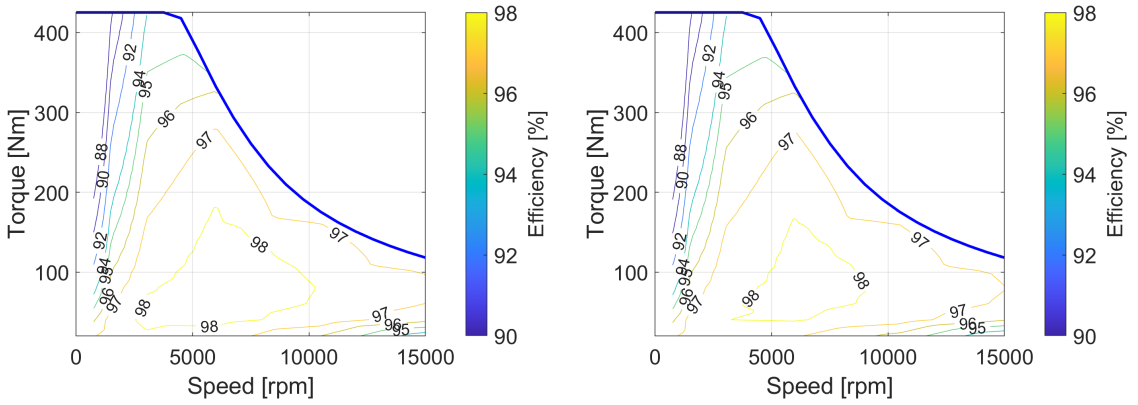

(a) Efficiency map with new operating points for EM with non-degraded material

(b) Efficiency map showing updated operating points for EM with degraded material

Figure 3.10: Efficiency maps with updated operating points using degraded and non-degraded material

The difference between the efficiencies range from 0.1 to 0.35 percentage points, seen in Figure 3.11.

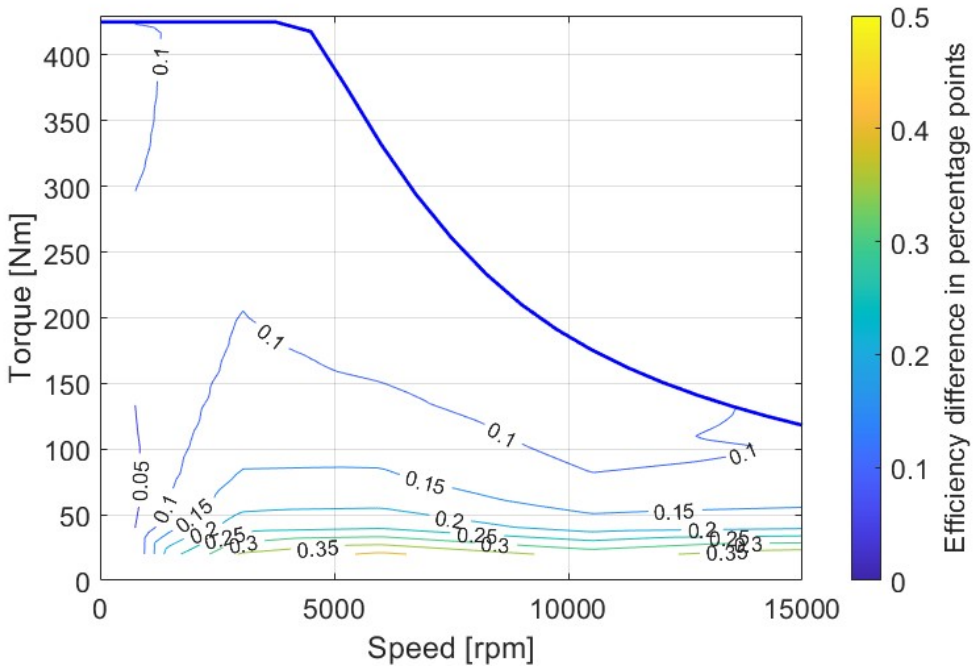

Figure 3.11: Difference in efficiency from non-degraded material versus degraded material simulation in percentage points

3.3.4.2 PWM feeding

To determine the losses with PWM feeding to the EM, different operating points were chosen and simulated with PWM. This was done due to the much more time-

consuming simulation that PWM has compared to sinusoidal feeding. The operating points where chosen to have a range of different speeds and different torque-levels to get a more comprehensive distribution and are shown in Table 3.6.

Table 3.6: Operating points for PWM simulation

Operating point	Ω [rpm]	i_d [A]	i_q [A]	T_e [Nm]
1	750	-23.7	91.3	40
2	750	-118.8	225.6	120
3	1500	-7.0	47.9	20
4	1500	-68.8	163.8	80
5	3000	-44.6	128.9	60

A graph with the operation points marked out in an efficiency map of the EM, using degraded materials, is visible in Figure 3.12.

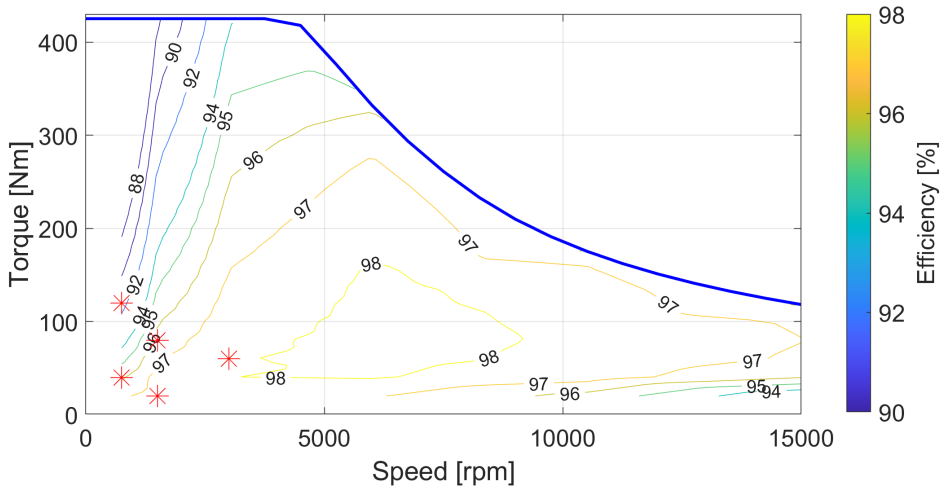

Figure 3.12: Efficiency map with degraded material and all operation points marked out

The simulation result of the iron losses were then compared to either non-degraded versus degraded material, to sinusoidal feeding to see how big impact the PWM feeding has, or to the actual EM to reveal how realistic the simulation was. The switching frequency was chosen to be the same as the machine measurement, which was 10 kHz. The input current and torque generated at operation point 5 is shown in figures 3.13 and 3.14. These have similar shapes with different current levels and different torque at the different operating points.

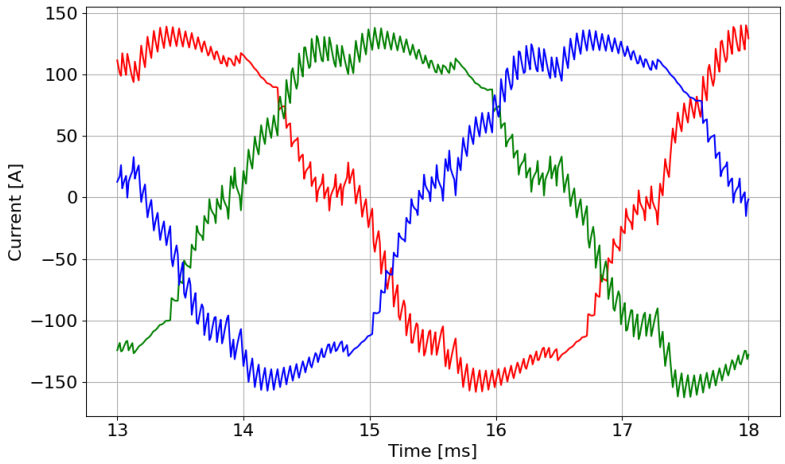

Figure 3.13: PWM input current signal to the EM at operation point 5

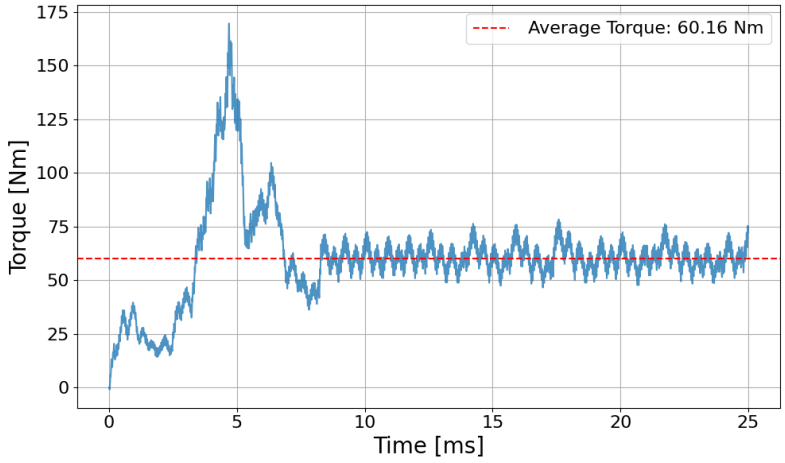

Figure 3.14: Torque generated at operation point 5

3.4 Drive cycle

To compare the impact of the different simulations in a more applicable manner a drive cycle was established for the operation points in Table 3.6, where different times were assigned to the different points. Operation point 1 has low torque and low speed, corresponding to cruising at low speed. Then the second point has high torque and low speed, like an acceleration case and therefore a shorter duration in the drive cycle. Third point is medium speed and low torque, cruising at a higher speed than the first point. Then the fourth point is akin to accelerating from the medium speed, before the last point being a high speed drive. The times used are presented in Table 3.7.

Table 3.7: Drive durations for all operation points

Operating point	Time at each point [s]
1	180
2	20
3	180
4	60
5	120

The durations were then used to calculate the energy by

$$E = \sum_{i=1}^{6} P_i \cdot t_i \tag{3.7}$$

where P_i is the power and t_i is the duration for each point, before calculating the efficiency as

$$\eta = \frac{E_{out}}{E_{in}} \tag{3.8}$$

where the energy in was the transmitted power times duration and the energy out used transmitted power minus the total losses instead.

4

Results

This chapter presents the results obtained to meet the objectives of the thesis, which focus on modeling iron losses due to manufacturing effects and comparing the impact of sinusoidal and PWM feeding. The results are divided into two main parts. Section 4.1 covers the outcomes of the model development, including the relative permeability model and the specific power loss model, both derived from material degradation measurements. Section 4.2 presents simulation results based on these models, including comparisons between sinusoidal and PWM feeding as well as between simulation and measured losses in an EM.

4.1 Model results

The modeling described in Section 3.2 was evaluated against measured values for all gathered data, both for the relative permeability modeling and the specific power loss modeling. The accuracy was assessed down to the same distance from the cut edge as the existing measurements since the extrapolation towards lower values could not be compared to any measurements.

4.1.1 Relative permeability model

To evaluate the relative permeability model (3.5) was used, and the results averaged over five different widths. This was done for a series of points and compared to the measurements at the same B values, as shown in Figure 4.1.

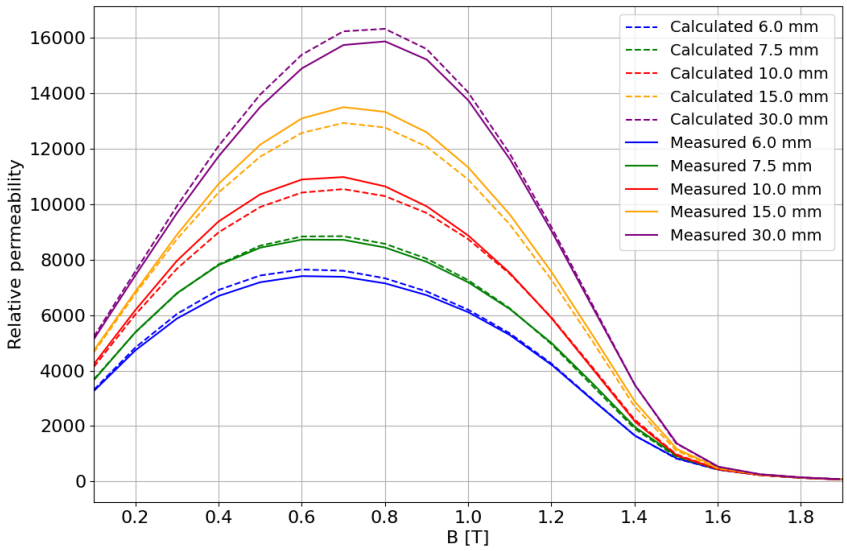

Figure 4.1: Measured and predicted relative permeabilities for different width of strips at 50 Hz

Comparing each measured point with its calculated value the deviation for the model was calculated to ensure the model was sufficiently accurate. The average deviation being between 1.5% and 3.7% was deemed tolerable, along with most maximum deviations being below 6%, except for one lone value for the 10 mm sample where it reached 9.0%. This was at the maximum flux density, 1.9 T and 50 Hz, where the relative permeability was very low so a small numerical deviation generated a larger deviation as a percentage. A summary of deviations is shown in Table 4.1.

Table 4.1: Maximum and average deviations for different sample widths for μ_r

Width of sample [mm]	Maximum deviation [%]	Average deviation [%]
6.0	3.92	1.98
7.5	5.14	1.51
10.0	9.03	3.66
15.0	5.70	3.40
30.0	3.26	1.95

Using the model for the relative permeability, the magnetic field strength was calculated as

$$H_{\text{calculated}} = \frac{B}{\mu_0 \mu_{r,\text{calculated}}} \tag{4.1}$$

enabling the generation of $B - H$ curves for further comparison and analysis along with being used in defining the materials used in the simulations. In Figure 4.2, both the measured and calculated $B - H$ curves are visible, showing that the model was capable of being used to calculate H-values as well.

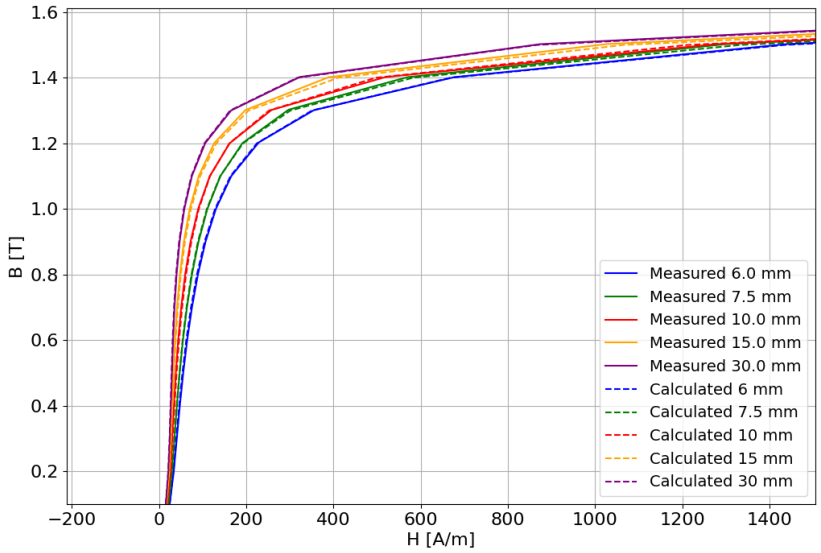

Figure 4.2: Measured and predicted H for different width of strips at 50 Hz

4.1.2 Specific loss model

For the specific loss model, P_s versus B curves were made to compare measurements and calculated values for five different distances from the cut edge. These are shown in Figure 4.3.

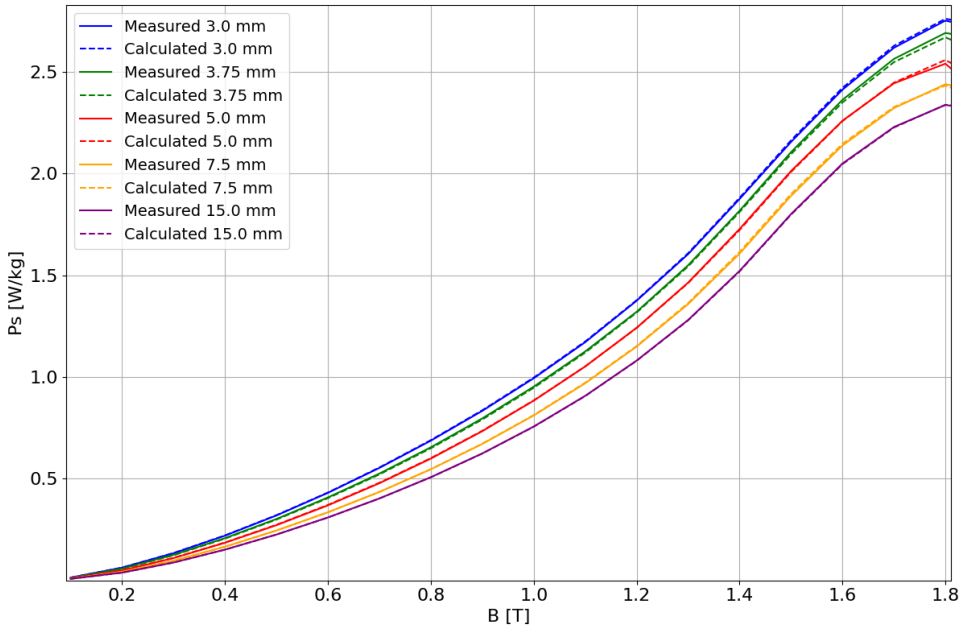

Figure 4.3: Calculated and measured P_s curves at 50 Hz

The deviations between calculations and measurements were calculated, showing great accuracy. In Table 4.2, the deviations are summarized.

Table 4.2: Maximum and average deviations for different sample widths for P_s

Width of sample [mm]	Maximum deviation [%]	Average deviation [%]
6.0	0.46	0.15
7.5	0.51	0.23
10.0	1.93	0.51
15.0	2.36	0.89
30.0	1.03	0.45

4.2 Simulation results

In this section, results from the FEM simulations on the EM will be presented, divided into different cases. The losses from the simulations with both non-degraded material, using material defined straight from the data sheet, and degraded material made with the degradation models, are compared when using sinusoidal feeding, as well as using PWM feeding. Then, the effect PWM feeding versus sinusoidal feeding had on the losses for the EM with degraded material. Another simulation case is comparing the core losses from the simulation with sinusoidal feeding and non-degraded material, with the losses from the simulations with the more realistic degraded material and PWM feeding. This is to visualize the increase in losses for the most advanced simulation versus the most simplified simulation. Lastly one machine measurement is compared to the simulation model in an attempt to give more credibility to the results.

4.2.1 Sinusoidal feeding

For the non-degraded sinusoidal simulations the core losses are visible in Figure 4.4. The maximum loss of 2.40 kW occurs at the operation point of 15 000 RPM and 118.09 Nm, where a high electrical frequency, due to the speed, and large magnetic flux density, due to the torque, lead to high hysteresis losses and eddy current losses as per (2.9).

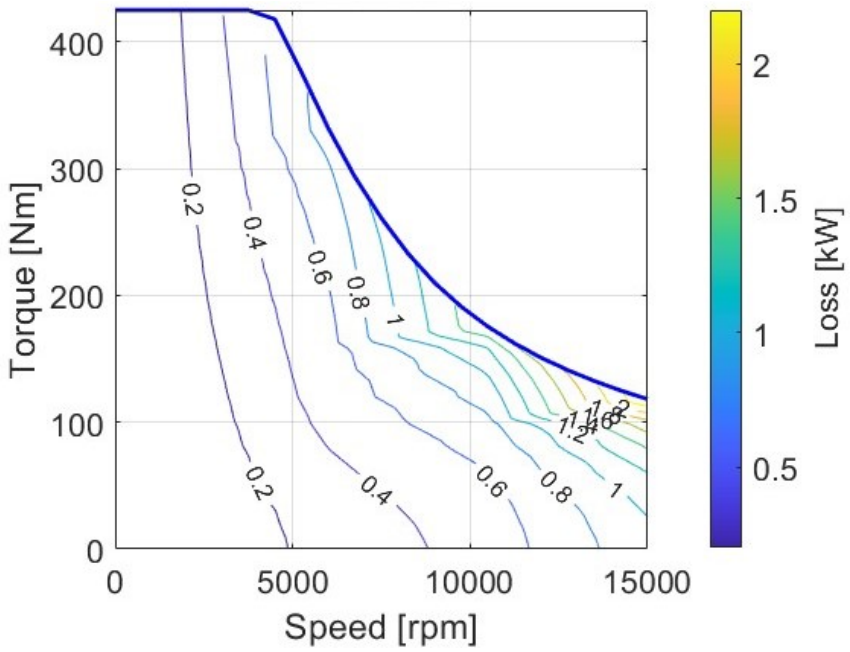

Figure 4.4: Iron losses in a torque map for the machine without degraded material

The total losses of the simulations with non-degraded material was heavily dictated by the stranded loss for the higher currents, as per (2.7). These total losses are shown in Figure 4.5.

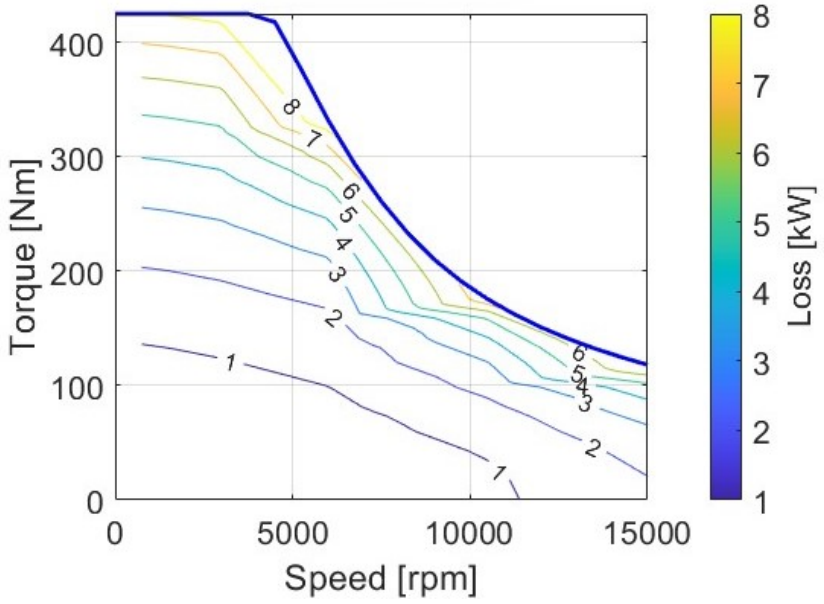

Figure 4.5: Total losses with no degradation in material

Introducing a degraded layer of material to the simulation increased core losses, the degraded core losses are seen in Figure 4.6.

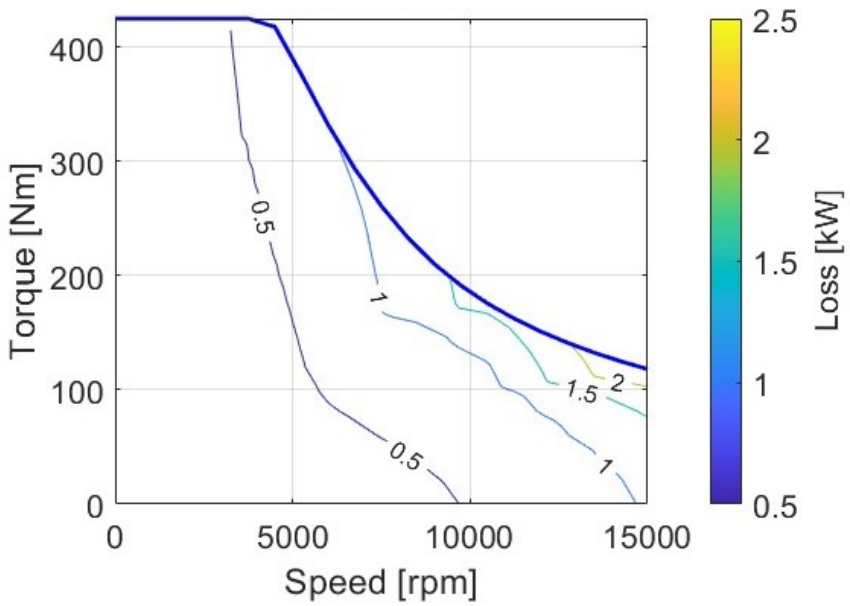

Figure 4.6: Iron losses in a torque map for the machine with degraded material

To visualize the difference as a percentage it was calculated by

$$\%_{increase} = 100 \cdot \frac{P_{fe,deg} - P_{fe}}{P_{fe}} \tag{4.2}$$

where $P_{fe,deg}$ is the core loss with a degraded material layer and P_{fe} is the core loss with non-degraded material. The core loss increased between 3 to 25%, and was higher for every point simulated. In Figure 4.7 the increase in losses as a percentage is mapped over the EM's operating range. The biggest percentage increase in iron losses are in the low to medium torque area, with speeds from 3000 rpm to 5000 rpm.

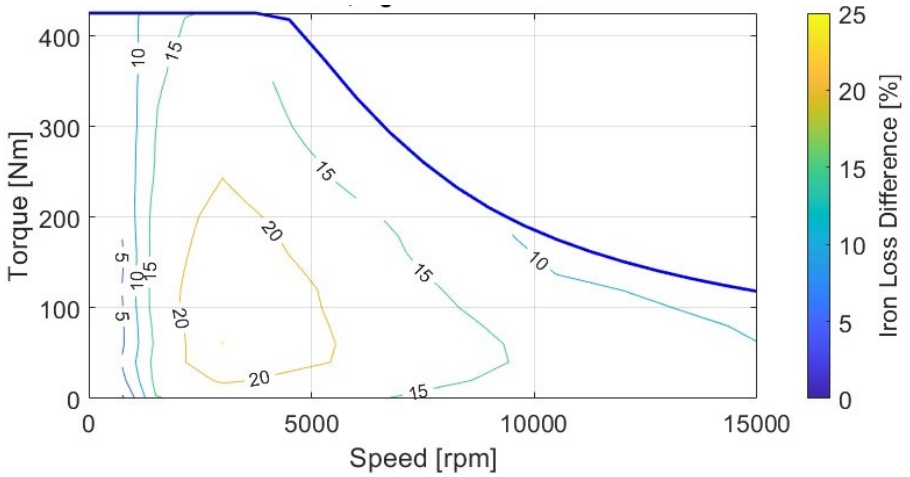

Figure 4.7: Degraded core losses increase over non-degraded core losses in percent

The values for the core losses from the five chosen operating points were extracted and presented in Table 4.3.

Table 4.3: Comparison of core losses for degraded versus non-degraded material EM with sinusoidal feeding

Operating point	Core losses non-degraded material [W]	Core losses degraded material [W]	Increase core loss in [%]
1	23.6	24.9	5.5
2	33.3	35.0	5.2
3	43.5	50.5	16.2
4	61.8	72.0	16.4
5	132.5	165.7	25.0

4.2.2 PWM feeding

For the first operating point, iron losses for the degraded material EM and the non-degraded material EM is visualized in Figure 4.8. The core loss graphs for the rest of the operation points is placed in Appendix A.

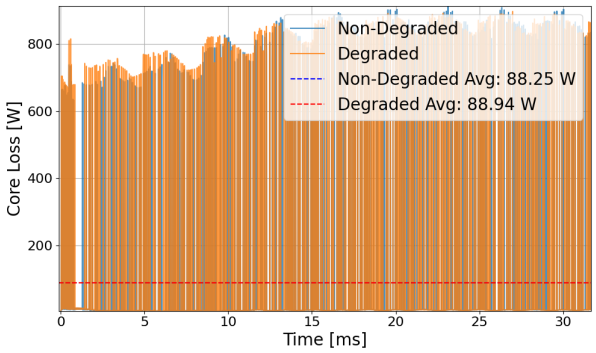

(a) Core loss at operation point 1 degraded versus non-degraded material

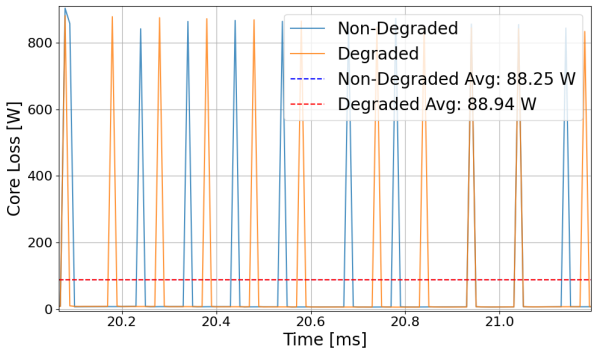

(b) Core loss zoomed

Figure 4.8: Core loss for degraded material versus non-degraded material with PWM feeding for operating point 1

From Table 4.4, it can be seen that the core losses increase at each operation point, similarly to the sinusoidal feeding case. The percentage increase in core losses between degraded and non-degraded material is smaller when using PWM feeding compared to sinusoidal feeding. This is likely because PWM already causes higher overall core losses. As a result, although degradation still increases the core losses, the relative increase is smaller under PWM, since the baseline loss is already higher compared to the sinusoidal case.

Table 4.4: Comparison of core loss for degraded versus non-degraded material EM with PWM-feeding

Operating point	Average core loss non-degraded material [W]	Average core loss degraded material [W]	Increase in core loss [%]
1	88.3	88.9	0.8
2	120.7	123.2	2.1
3	130.3	138.9	6.6
4	174.0	185.6	6.7
5	352.3	377.9	7.3

In Table 4.5, the total losses calculated are the core losses added with the copper losses, calculated from (2.7). The copper losses are the same for the degraded versus non-degraded case for each point, making the only difference between each case the core losses. This is why the percentage increase in total losses is smaller than the percentage increase in core losses, the overall total is larger, but the actual increase is only in the core losses so it makes up a smaller part of the total.

Table 4.5: Comparison of total losses for degraded versus non-degraded material EM with PWM-feeding

Operating point	Total losses non-degraded material [W]	Total losses degraded material [W]	Increase in total loss [%]
1	193.6	194.3	0.4
2	891.0	893.5	0.3
3	158.0	166.7	5.5
4	548.0	559.6	2.1
5	575.1	600.7	4.5

To calculate the total efficiency decrease due to degradation with PWM feeding, the total losses are subtracted from the transmitted power, then divided by the transmitted power, as shown in (4.3), where the results of this are disclosed in Table 4.6. There it can be seen that the degradation has an effect on the total efficiency, where a decrease goes from 0.02 percentage points up to 0.28 percentage points.

$$\eta = \frac{P_{trans} - P_{loss,tot}}{P_{trans}} \tag{4.3}$$

Table 4.6: Comparison of efficiency for degraded versus non-degraded material EM with PWM-feeding

Operating point	Efficiency non-degraded material [%]	Efficiency degraded material [%]	Efficiency decrease in percentage points
1	93.83	93.81	0.02
2	90.54	90.51	0.03
3	94.97	94.69	0.28
4	95.63	95.54	0.09
5	96.95	96.81	0.14

4.2.3 Sinusoidal versus PWM feeding

When comparing sinusoidal versus PWM feeding, the degraded material in the EM was used for both sinusoidal and PWM feeding. The same method to calculate the total losses and efficiency was used as in section 4.2.2. The effect of PWM feeding on core losses from the simulations are much higher than the degradation, as seen from Table 4.7, where the biggest increase in percent is 257.9%. A trend to the core losses are that as the speed increases, the increase in core loss in percent decrease. This is only for these five operation points, as when the speed increases over 3000 rpm, this trend might not be correct. A visualization of the core losses are seen in Figure 4.9, where the PWM fed simulation has filtered core losses, to more easily compare the sinusoidal feeding.

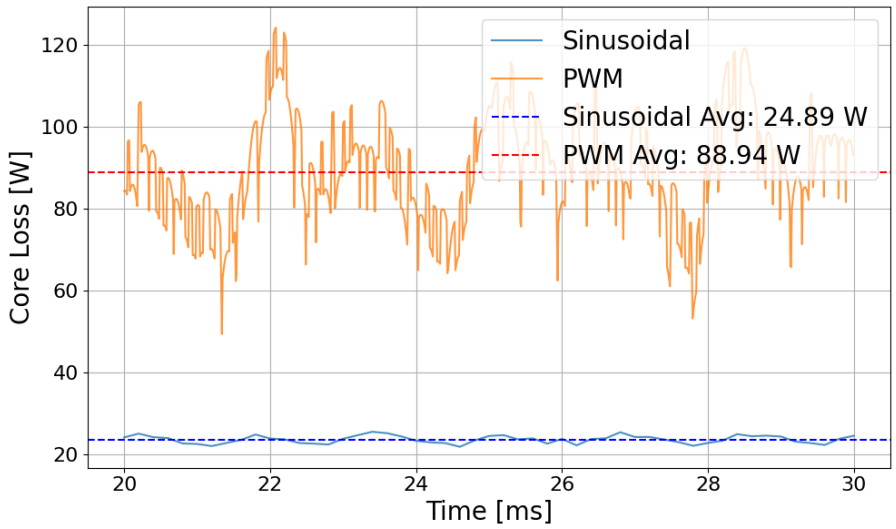

Figure 4.9: Sinusoidal core loss with degraded material simulation versus PWM filtered core loss with degraded material simulation at operation point 1

Table 4.7: Comparison of core losses with either sinusoidal or PWM feeding

Operating point	Average core loss sinusoidal feeding [W]	Average core loss PWM feeding [W]	Increase in core loss [%]
1	24.9	88.9	257.9
2	35.0	123.2	251.6
3	50.5	138.9	175.0
4	72.0	185.6	157.8
5	165.7	377.9	128.0

The total loss increase, as seen in Table 4.8, are quite similar except for operation point 2 and 3. For point 2, the torque is the highest that was simulated, meaning the RMS value of the current is the largest, leading to the highest copper losses. This means that the increase in core losses due to PWM are not as big fractionally compared to other operating points. The same reasoning could be done for operating point 3, but the opposite as the torque is the lowest, leading to lowest RMS current values and lower copper losses. The core losses then make up a larger part of the total losses and an increase in core losses is more noticeable.

Table 4.8: Comparison of total losses with either sinusoidal or PWM feeding

Operating point	Total losses sinusoidal feeding [W]	Total losses PWM feeding [W]	Increase in total loss [%]
1	130.2	194.3	49.2
2	805.4	893.5	10.9
3	78.3	166.7	113.0
4	446.0	559.6	25.5
5	388.9	600.7	54.6

The decrease in efficiency is much more apparent for the PWM feeding versus sinusoidal feeding, compared to efficiency lost due to degradation, visible in Table 4.9. From the simulations, the lowest decrease in efficiency is still 0.9%, with operation point number 3 being at 2.8% decrease in efficiency. This shows the big difference in sinusoidal versus PWM feeding.

Table 4.9: Comparison of efficiency with either sinusoidal or PWM feeding

Operating point	Efficiency sinusoidal feeding [%]	Efficiency PWM feeding [%]	Efficiency decrease in percentage points
1	95.6	93.8	2.0
2	91.4	90.5	0.9
3	97.5	94.7	2.8
4	96.5	95.6	0.9
5	97.9	96.8	1.2

4.2.4 Sinusoidal feeding with non-degraded material versus PWM feeding with degraded material

These simulation results were compared as the non-degraded material simulation with sinusoidal feeding is the model that is the simplest and least realistic whereas the degraded material with PWM feeding is the simulation with the most realistic model that was built. This is to see how wrong the estimation for the simplest model is, especially for core losses, resulting in a combination of degradation effects and PWM feeding losses.

From Table 4.10, it is shown that the core losses increased significantly, similar to the sinusoidal degraded material simulation versus PWM degraded material. When comparing Table 4.10 with Table 4.7, the increase in core loss percentage is not that big. This is due to the losses being so heavily dictated by the PWM feeding.

Table 4.10: Comparison of core losses with sinusoidal feeding with non-degraded material versus PWM feeding with degraded material

Operating point	Average core loss sinusoidal feeding [W]	Average core loss PWM feeding [W]	Increase in core loss [%]
1	23.6	88.9	276.7
2	33.3	123.2	270.0
3	43.5	138.9	219.3
4	61.8	185.6	200.3
5	132.5	377.9	185.2

The results from Tables 4.11 and 4.12 are similar to the degraded material sinusoidal feeding case, with an expected slight increase in losses and lower efficiency. This means that when one wants to simulate an EM quickly, without considering degradation of the material, when connected to PWM, similar results to the more realistic simulation is achievable.

Table 4.11: Comparison of total losses with sinusoidal feeding with non-degraded material versus PWM feeding with degraded material

Operating point	Total losses sinusoidal feeding [W]	Total losses PWM feeding [W]	Increase in total loss [%]
1	128.9	194.3	50.7
2	803.7	893.5	11.7
3	71.2	166.7	134.1
4	435.9	559.6	28.4
5	355.3	600.7	69.1

Table 4.12: Comparison of efficiency with sinusoidal feeding with non-degraded material versus PWM feeding with degraded material

Operating point	Efficiency sinusoidal feeding [%]	Efficiency PWM feeding [%]	Efficiency decrease in percentage points
1	95.9	93.8	2.1
2	91.5	90.5	1.0
3	97.7	94.7	3.0
4	96.5	95.6	1.1
5	98.1	96.8	1.3

4.2.5 Drive cycle analysis

The losses for each simulation case was used in the drive cycle analysis to get the total efficiency over the cycle, seen in Table 4.13, where the simulations using sinusoidal feeding and non-degraded material had the best efficiency due to it having the lowest losses. The simulations with PWM feeding and degraded material had the worst efficiency, being 1.46 percentage points lower than the best case. The difference between using non-degraded material or degraded material was similar for both feeding type, where the difference for the PWM feeding was 0.12 percentage points and 0.14 percentage points for the sinusoidal feeding.

Table 4.13: Efficiency over the whole drive cycle for the different simulation setups

Simulation type	**Efficiency over whole drive cycle**
Sinusoidal feeding with non-degraded material	97.29%
Sinusoidal feeding with degraded material	97.15%
PWM feeding with non-degraded material	95.95%
PWM feeding with degraded material	95.83%

4.2.6 Machine measurement versus simulation

For the simulation, the model used was the degraded material with PWM feeding, as the machine was fed with PWM, making the comparison the most similar to the real machine. When running the machine at 3000 rpm at no-load, smaller currents are still drawn from the machine. The average of these currents are described in Table 4.14. These currents are then used as input into the simulated model, to replicate as much as possible for the simulation.

Table 4.14: i_d and i_q at machine no-load measurement at 3000 rpm

i_d [A]	i_q [A]
2.14	0.19

In Figure 4.10, it can be seen that the simulated model had an average core loss of

326.0 W, close to the measured loss of the machine at 361.3 W, where stranded loss was subtracted from the total loss of the machine. It still includes friction losses that are not included in the simulation which should increase the difference. The difference in percent is

$$\%_{difference} = \frac{P_{fe,average,measured} - P_{fe,average,simulated}}{P_{fe,average,measured}} = 6.7\% \tag{4.4}$$

which means the simulation of the degraded material with PWM feeding was realistic for this operation point. To evaluate the model fully, more operating points need to be studied to see how core losses for other points match with the real machine.

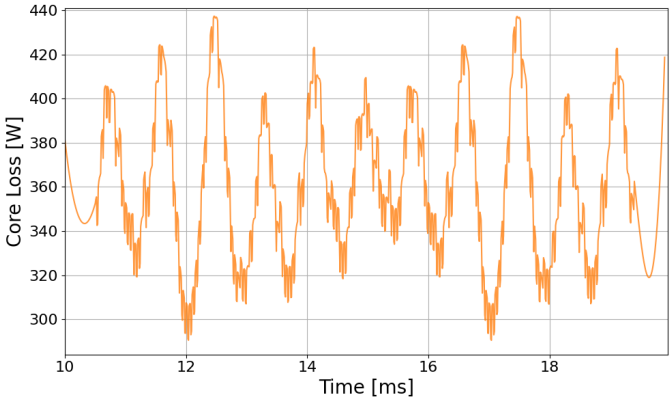

(a) Simulated core loss at 3000 RPM under no-load operation, $P_{fe,average,simulated}$=361.3 W

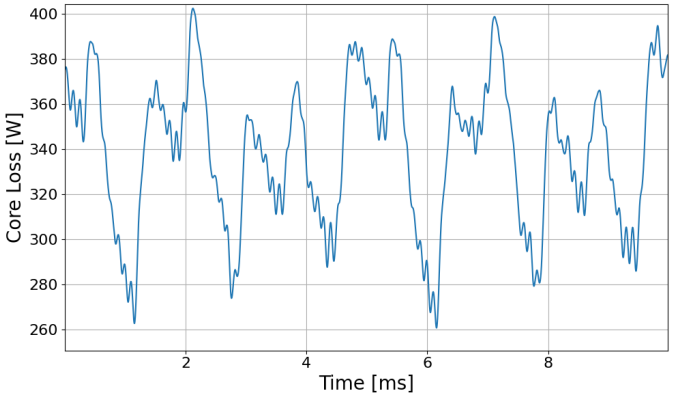

(b) Measured core loss at 3000 RPM under no-load operation, $P_{fe,average,measured}$=338.7 W

Figure 4.10: Simulated PWM with degraded material versus measurements from actual EM, both at 3000 RPM under no-load operation

4.2.7 Battery voltage effect on PWM losses

The effect different battery voltages had on the core losses was also examined, where different voltages will lead to different timings for the PWM switching schedule. Therefore the PWM simulation for 0 Nm and 3000 RPM was ran four times with different voltages, seen in Table 4.15, to examine the trend.

Table 4.15: Different battery voltages used for no-load simulations

Voltage [V]	210	290	380	460

There was a clear trend in the simulations, where the lower voltages led to lower losses. Fitting a curve to the simulated points gives a relation between the voltage and core loss, where the slope is 0.72 and an interception at 32.6, but that is mathematical. With no voltage applied there would be no excitation in the machine and no losses.

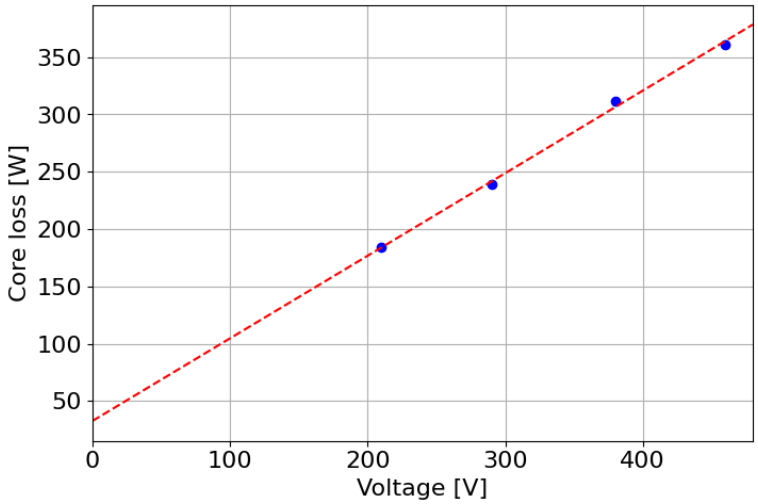

Figure 4.11: Simulated core loss at no-load operation and 3000 RPM with different battery voltages

5
Discussion

5.1 Modeling

The modeling used in this thesis was used to define materials in FEM-based simulations that showed promise. The magnetic properties worsened closer to the cut edge and the losses increased. The full extent of how well the modeling works needs to be studied more to draw any real conclusions on its validity.

Due to the widths of strips available, the modeling is fully based on values gathered for distances between 3 to 15 mm from the cut edge, so to model closer than 3 mm the results will be extrapolated. For example by looking at the specific power loss in Figure 2.16 it increases exponentially closer to the cut edge. To validate the model further more measurements on thinner strips should be done to compare with the modeling.

Creating fewer thicker degraded layers with the model avoids extrapolating, defining materials with lower loss but higher volume. On the other hand when modeling many thin layers the specific power loss will be higher closest to the cut edge but a lower volume will lead to less total loss. Which one generates more realistic results was not examined, but is of high interest.

Looking at the parameters for the relative permeability modeling in Figure 3.3, there is a general trend until 1.3 T where all parameters rapidly change. Since a_p and c_p in (2.12) are both in front of exponentials they are intertwined, and when a_p increases c_p decreases. Therefore the rise in a_p at 1.3 T might be unnecessary and a a_p-value closer to the one at 1.2 T would generate a smoother curve for c_p without a large loss of accuracy. The expression used, (2.12), is also just one possible solution, another expression could provide a better fit.

5.2 Simulation

When comparing degraded and non-degraded material under sinusoidal feeding, the outcome was as expected. The iron losses increased between 3 and 25% from the non-degraded to degraded case. This result is similar to [5] where the result of degradation went up to 24.1%, indicating the simulations to be accurate.

When comparing sinusoidal feeding and PWM feeding simulations, the difference in iron losses were a lot higher for the PWM feeding, where one thing believed to have increased the losses is the ripple in the input current creating minor hysteresis loops. The effect of PWM is obvious, and has a much larger impact than the degradation effect for all operation points simulated. For the non-degraded material sinusoidal feeding versus the degraded material PWM feeding, the losses in percent does not increase that much, when compared to the degraded material sinusoidal feeding simulation. This is due to the higher fraction of loss coming from PWM simulations, meaning the degradation effects are not as dominant.

The PWM simulation with degraded material iron losses compared to the machine measurements are quite similar for the operating point simulated, no-load operation at 3000 RPM. This indicates that the model has promise, but more studies need to be done at different operating points to draw a conclusive answer. It would be interesting to test a machine with a load to see how the simulated model would compare. One aspect that was different was the different PWM methods used. For the real machine, SVPWM was used and in the simulations, SPWM was used. If SVPWM was used the difference might decrease. The comparison also does not include the friction losses in the real machine measurements, skewing the results a small bit. The best way to eliminate this source of error would be to measure the friction losses on the real machine and subtract this, to isolate the iron losses. This is because Ansys Maxwell does not include and does not have an obvious way to include friction losses to the system.

5.3 Ethics and sustainability

As described in the introduction, the electric vehicle industry is growing rapidly. The demand for high efficiency EMs is high, making accuracy on simulations essential. In order to design realistic EMs with correct efficiency,a high demand for simulation accuracy is necessary. From a sustainability perspective, high accuracy simulations are important to minimize the environmental impact. From an ethical standpoint, transparency from the business designing EMs is essential to build trust from consumers.

Modeling iron losses correctly is also important from both ethical and sustainability perspectives, as understanding how iron losses vary could contribute to reducing losses when designing EMs. Having accurate simulation models make it so EM designs can be evaluated without having to build the actual machine and more designs can be compared before one is chosen and built, instead of having to manufacture multiple designs. Reducing losses would also increase efficiency, leading to less energy waste, and ultimately less energy used per EM.

6
Conclusion

The purpose of this thesis was to model the effects of degradation of iron losses due to manufacturing effects and due to both sinusoidal and PWM feeding. This was realized by measuring the degradation effects on steel sheets, to model a degradation function to create $B-H$ curves which later was implemented into materials in the FEM based software Ansys Maxwell. The PWM feeding was built using Ansys Simplorer, then connected through Ansys Twin Builder. Furthermore, simulations with similar conditions were done to compare to a real machine. When this was completed, comparisons were made and conclusion of how iron losses differ during different conditions were drawn.

The functions developed in the degradation modeling made it possible to create materials with degraded magnetic properties in line with how those properties degraded in the single strips, for any distance from the cut edge. This was compared to the measured values for the strips where the average deviation for the permeability model was within 3.7% from the measured values, and the specific power loss model was within 0.9% from the measurements. Therefore the models were considered accurate and used to model a degraded layer of material with a distance of 3 mm to the cut edge, and implemented in the model.

When looking at the degradation effects due to manufacturing with the sinusoidal fed simulation, the core loss increased at every point simulated over the EM's operating range, where the increase of core loss ranged from 3 to 25%. For the PWM fed simulations, five different operating points were simulated, with both degraded material and non-degraded material. The increase in core loss ranged from 0.8 to 7.3%, which resulted in an increase of 0.3 to 5.5% in total losses. The increase in total losses resulted in a decrease in efficiency due to degradation from the PWM fed simulation to between 0.02 to 0.28 percentage points. When comparing sinusoidal feeding with PWM feeding for the degraded material EM, the increase in core loss were between 128 to 257.9%, resulting in an increase in total losses of 10.9 to 113.0%. The decrease in efficiency for these five operating points ranged from 0.9 to 2.8 percentage points. When combining the effects of degradation and PWM feeding, the simulation with the EM with non-degraded material fed with sinusoidal feeding was compared to the degraded material PWM fed EM. The core losses increased for the PWM degraded material case by 185.2 to 276.7%, resulting in a total loss increase of 11.7 to 134%. The efficiency decrease due to PWM and degradation ranged from 1.0 to 3.0 percentage points, where the effect from PWM feeding contributed more than the degradation.

For the drive cycle simulations, the degraded material PWM fed EM was had the worst efficiency, being 1.46 percentage points lower than the highest efficiency, being the sinusoidal fed non-degraded EM. The difference between using degraded material and non-degraded resulted in a decrease in efficiency similar for the sinusoidal fed and PWM fed simulations, being a decrease of 0.14 percentage points for the sinusoidal feeding and a decrease of 0.12 percentage points for the PWM feeding. When comparing the degraded material PWM fed EM simulation to a real machine measurement, the average core losses were 361.3 W for the simulation and 338.7 W for the machine measurement, leading to an error of 6.7% between simulation and a real machine.

7
Future Work

To gain a deeper understanding of the degradation of material in EMs, one could examine different steps in the process to create a stator. For instance, measuring the magnetic properties of a stator with windings and a dummy rotor, could further reveal the effects of degradation. This could serve as a stepping stone between sheet and full machine. Additionally, a more physical meaning to the specific loss modeling would be interesting, enabling loss separation to see how the different parts of iron losses is affected by degradation. For the simulation, a better circuit could be built with current controllers using different techniques to have faster and better responses to disturbances. Another thing is building a circuit with SVPWM instead of SPWM to get closer to the measured machine setup. It would also be interesting to investigate using more and smaller layers of degradation, closer to the cut edge. Furthermore, accounting for the degradation in the rotor should be considered during simulation to more accurately simulate iron losses. The drive cycle analysis performed only included five drive points, a more comprehensive drive cycle analysis like the Worldwide Harmonized Light-Duty Vehicles Test Procedure (WLTP) [23] would be useful as it is a more standardized way to evaluate EM's. Finally, comparing simulations with a machine operating under load conditions would widen the range of the models validity.

References

[1] IEA, "Trends in electric cars – global ev outlook 2024 – analysis," 2024, accessed: 6 Mar. 2025. [Online]. Available: https://www.iea.org/reports/global-ev-outlook-2024/trends-in-electric-cars

[2] S. Soltanipour, T. Thiringer, and J. Lindström, "Battery electric vehicle performance evaluation by considering punching effect on pmsm iron cores," in *2022 International Conference on Electrical Machines (ICEM)*, 2022, pp. 2162–2168.

[3] M. Oka, H. Kiyotake, M. Enokizono, and D. Wakabayashi, "Iron loss measurements under pwm excitation for ring cores made of ultrathin electrical steel sheets for a stator core," in *2020 International Conference on Electrical Machines (ICEM)*, vol. 1, 2020, pp. 2294–2300.

[4] *IEC 60404-2*, The International Electrotechnical Commission Std., 2008.

[5] U. Einarsson and E. Nygren, "Iron loss modelling and material property degradation: Effects of cutting techniques, material variations, and sinusoidal vs. non-sinusoidal flux distribution," Master's thesis, Chalmers University of Technology, Gothenburg, Sweden, 2024, master's Thesis, Department of Electrical Engineering.

[6] Z. Gmyrek, A. Cavagnino, and L. Ferraris, "Estimation of the Magnetic Properties of the Damaged Area Resulting From the Punching Process: Experimental Research and FEM Modeling," *IEEE Transactions on Industry Applications*, vol. 49, no. 5, pp. 2069–2077, Sep. 2013. [Online]. Available: https://ieeexplore.ieee.org/document/6511985/

[7] X. Chen, H. Wu, J. D. Ede, G. W. Jewell, L. M. Jones, and H. Ghadbeigi, "A model to account for magnetic permeability changes resulting from edge damage caused by laser cutting in a high performance cobalt-iron alloy," *Journal of Magnetism and Magnetic Materials*, vol. 584, p. 171081, Oct. 2023. [Online]. Available: https://www.sciencedirect.com/science/article/pii/S030488532300731X

[8] H. Naumoski, B. Riedmüller, A. Minkow, and U. Herr, "Investigation of the influence of different cutting procedures on the global and local magnetic properties of non-oriented electrical steel," *Journal of Magnetism and Magnetic Materials*, vol. 392, pp. 126–133, Oct. 2015. [Online]. Available: https://www.sciencedirect.com/science/article/pii/S0304885315301554

[9] M. Bali, H. D. Gersem, and A. Muetze, "Finite-element modeling of magnetic material degradation due to punching," *IEEE Transactions on Magnetics*, vol. 50, no. 2, pp. 745–748, 2014.

[10] R. Sundaria, A. Lehikoinen, A. Arkkio, and A. Belahcen, "Effects of Manufacturing Processes on Core Losses of Electrical Machines," *IEEE*

Transactions on Energy Conversion, vol. 36, no. 1, pp. 197–206, Mar. 2021. [Online]. Available: https://ieeexplore.ieee.org/document/9106797/

[11] Koprivica, A. Milovanovic, and M. Plazinić, "Standard methods of measurement of the magnetic properties of electrical steel strip and sheet," *Journal Name*, Nov. 2012.

[12] B. Zhang and D. Qiu, *m-Mode SVPWM Technique for Power Converters*, ser. Springer eBooks. Springer, 2019, accessed via Chalmers Library E-book Collection.

[13] S.-H. Kim, *Electric Motor Control*, 2017.

[14] W. Zhang, H. Li, and J. Wang, "Research on carrier-based pwm with zero-sequence component injection for vienna type rectifiers," *IEEE Transactions on Power Electronics*, vol. 36, no. 10, pp. 11 450–11 459, 2021.

[15] S.-H. Park, E.-C. Lee, J.-C. Park, S.-W. Hwang, and M.-S. Lim, "Prediction of Mechanical Loss for High-Power-Density PMSM Considering Eddy Current Loss of PMs and Conductors," *IEEE Transactions on Magnetics*, vol. 57, no. 2, pp. 1–5, Feb. 2021. [Online]. Available: https://ieeexplore.ieee.org/document/9133579/

[16] A. Krings, S. Nategh, A. Stening, H. Grop, O. Wallmark, and J. Soulard, "Measurement and modeling of iron losses in electrical machines," 01 2012, pp. 101–119.

[17] A. Krings, "Iron losses in electrical machines - influence of material properties, manufacturing processes, and inverter operation," Ph.D. dissertation, KTH, School of Electrical Engineering (EES), Electrical Energy Conversion, Sweden, 2014, doctoral thesis, monograph (Other academic). [Online]. Available: https://www.diva-portal.org/smash/get/diva2:717326/FULLTEXT01.pdf

[18] E. Campara and A. Solokovic, "Iron loss modelling for a permanent magnet synchronous motor," Master's thesis, Chalmers University of Technology, Sweden, 2020, master's Thesis in Electric Power Engineering (MPEPO), MSc. [Online]. Available: https://hdl.handle.net/20.500.12380/301805

[19] V. Leivsdottir, "Investigation of loss calculation methods for pmsms and implementation of loss functionality on a developed fem model," Master's thesis, Norwegian University of Science and Technology, 2016, master's Thesis.

[20] G. Mörée and M. Leijon, "Iron loss models: A review of simplified models of magnetization losses in electrical machines," *Journal of Magnetism and Magnetic Materials*, vol. 609, p. 172163, 2024. [Online]. Available: https://www.elsevier.com/locate/jmmm

[21] U.-J. Seo, D.-J. Kim, Y.-D. Chun, and P.-W. Han, "Mechanical cutting effect of electrical steel on the performance of induction motors," *Energies*, vol. 13, no. 23, 2020. [Online]. Available: https://www.mdpi.com/1996-1073/13/23/6314

[22] Brockhaus Measurements, *MPG-Expert 3 - Manual*, Brockhaus Measurements, 2018.

[23] United Nations Economic Commission for Europe, "Proposal for a new un regulation on the worldwide harmonized light vehicles test procedure (wltp)," https://unece.org/DAM/trans/doc/2014/wp29/ECE-TRANS-WP29-2014-027e.pdf, 2014, accessed: 2025-05-30.

A

Appendix

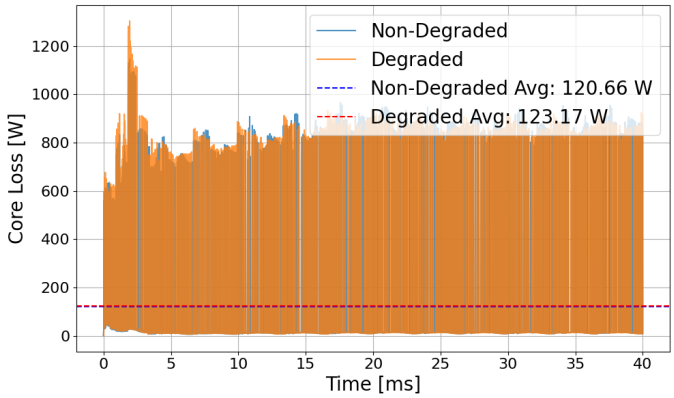

(a) Core loss at operation point 2 degraded versus non-degraded material

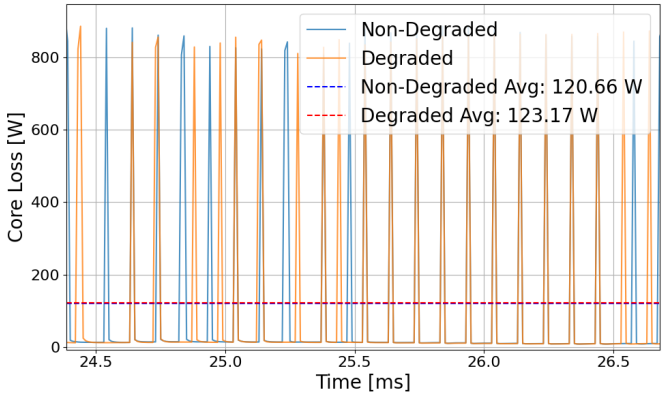

(b) Core loss zoomed

Figure A.1: Core loss for degraded material versus non-degraded material PWM feeding for operating point 2

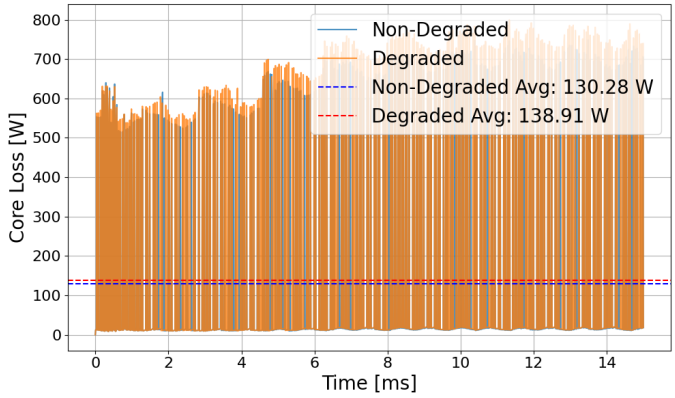

(a) Core loss at operation point 3 degraded versus non-degraded material

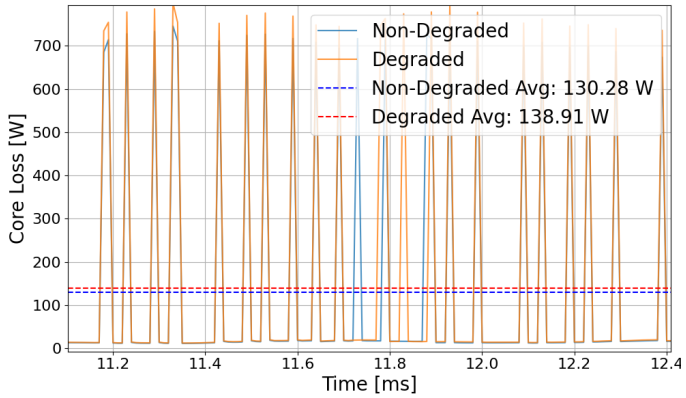

(b) Core loss zoomed

Figure A.2: Core loss for degraded material versus non-degraded material PWM feeding for operating point 3

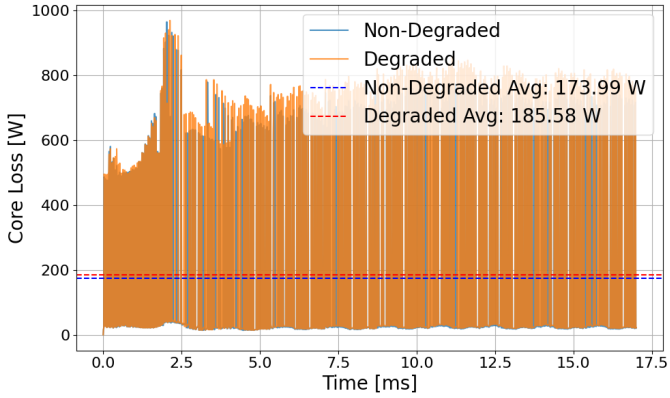

(a) Core loss at operation point 4 degraded versus non-degraded material

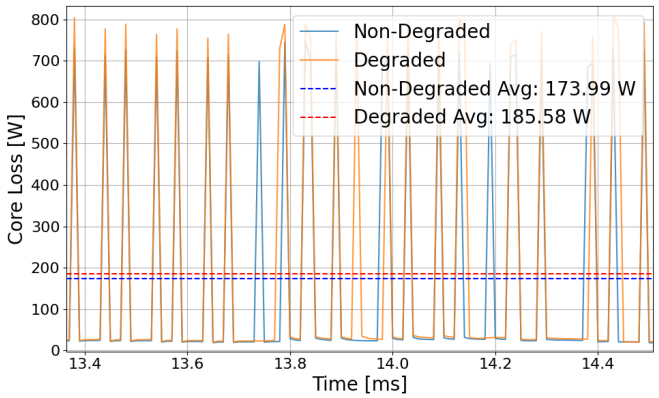

(b) Core loss zoomed

Figure A.3: Core loss for degraded material versus non-degraded material PWM feeding for operating point 4

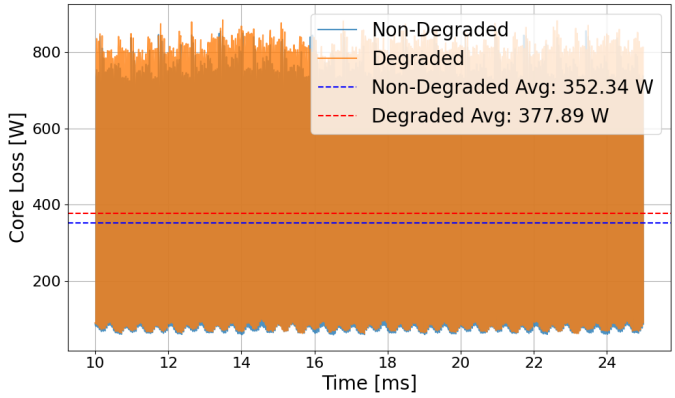

(a) Core loss at operation point 5 degraded versus non-degraded material

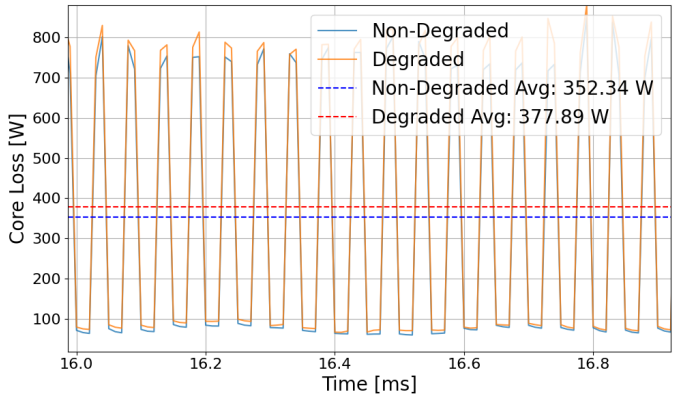

(b) Core loss zoomed

Figure A.4: Core loss for degraded material versus non-degraded material PWM feeding for operating point 5

DEPARTMENT OF ELECTRICAL ENGINEERING
CHALMERS UNIVERSITY OF TECHNOLOGY
Gothenburg, Sweden
www.chalmers.se

CHALMERS
UNIVERSITY OF TECHNOLOGY